THESIS

METABOLIC INTERVENTIONS IN THE TREATMENT OF MYCOBACTERIUM TUBERCULOSIS INFECTION

Submitted by

David Ackart

Department of Microbiology, Immunology and Pathology

In partial fulfillment of the requirements

For the Degree of Master of Science

Colorado State University

Fort Collins, Colorado

Summer 2023

Master's Committee:

Advisor: Randall Basaraba

Brendan Podell
Adam Chicco

ABSTRACT

METABOLIC INTERVENTIONS IN THE TREATMENT OF MYCOBACTERIUM TUBERCULOSIS INFECTION

Tuberculosis remains a global threat. For the first time in over a decade, there was an increase in deaths in 2021. Current antimicrobial treatments are lengthy and costly, which leads to non-compliance. Host-directed therapies have emerged as a possible adjuvant to antimicrobial treatment. It has become clear that immune cell function and metabolic pathways are intertwined and a target for therapy. Previously, metformin, a partial inhibitor of complex I, was associated with decreased disease burden in the guinea pig model. Based on these findings, we hypothesized that limiting glycolysis would reduce lesion burden and bacterial viability. To test our hypothesis, we infected guinea pigs for thirty days and then administered metformin or 2-deoxy-glucose alone, and in combination. After 90 days of infection, histological analysis revealed increased healing in the combination treatment. To determine the effect of treatment on cellular metabolism, we evaluated treatments in guinea pig bone marrow-derived macrophages. We found that the combination treatment reduced bacterial viability, prevented mitochondrial damage, and increased apoptosis, which helps support *in vivo* findings. These findings suggest that the metabolic switch of immune cells to glycolysis alone is insufficient to control *Mycobacterium tuberculosis* infection; it is essential, as is oxidative phosphorylation.

ACKNOWLEDGMENTS

I am deeply indebted to Dr. Randall Basaraba and Dr. Brendan Podell for their unwavering support and guidance throughout my master's program. In my role as a student and employee, their expertise, patience, generosity, and flexibility have been invaluable to me personally and are crucial in my success and the success of my studies.

I would also like to thank Dr. Adam Chicco for serving on my thesis committee and providing valuable feedback and suggestions. His insights and guidance were instrumental in shaping my research and writing this thesis.

Special thanks to my wife, Heather, for being my inspiration and motivation before, through, and after these years of graduate study. Daughters Aviendha and Raedyn, and parents Frances and David, I am forever grateful for the love and support. I especially want to thank my Uncle George and Aunt Darlene for their commitment to my education.

Finally, my gratitude to the current and former laboratory members who make this journey enjoyable and rewarding.

TABLE OF CONTENTS

INTRODUCTION AND LITERATURE REVIEW

I. Tuberculosis

Mycobacterium tuberculosis, the causal agent of tuberculosis, remains a leading infectious disease killer worldwide, disproportionately affecting developing nations [1]. The World Health

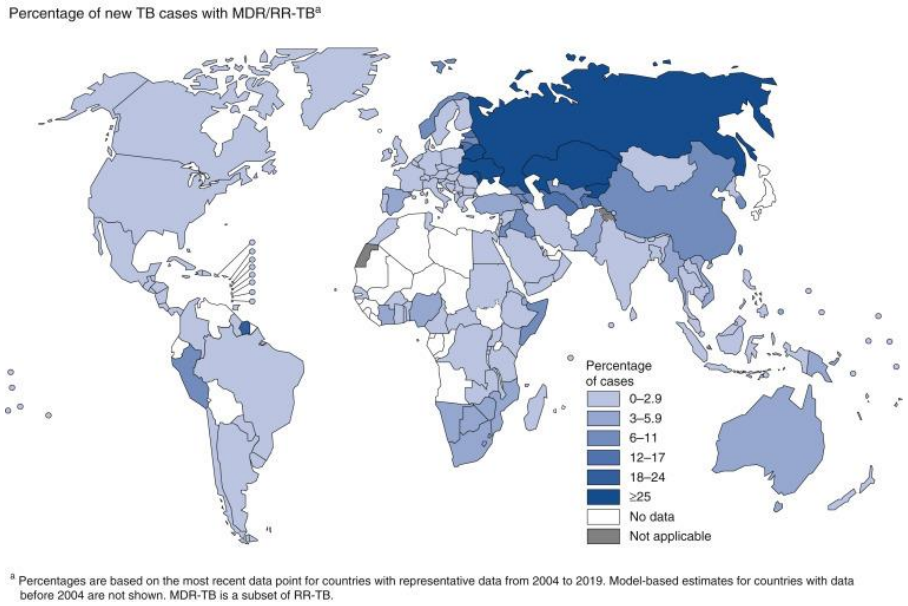

Figure 1.1. New cases of drug-resistant tuberculosis World Health Organization. *Global Tuberculosis Report, 2019*. Geneva, Switzerland: WHO; 2019. [2]

Organization estimates that a quarter of the world's population is currently infected. Last year alone, approximately 1.5 million people succumbed to the disease [1].

Drug resistance is an ever-increasing problem with multidrug-resistant and extensively drug-resistant strains. Currently, just over half of the world's multidrug-resistant tuberculosis cases go untreated. Moreover, extensively drug-resistant tuberculosis has been identified in 131 countries and has a successful treatment rate of 30% [1, 3, 4]. In addition to drug resistance, predisposing factors to disease exasperate the spread of *M. tuberculosis*. The most significant risk factor is HIV/AIDS, which increases the risk of contracting tuberculosis by 20 times. Moreover, diabetes mellitus affects 422 million people worldwide, and 15% of all tuberculosis cases are tied to diabetes as of 2014 [1].

Current treatments are lengthy, expensive, and difficult to monitor compliance worldwide. With only three treatments reaching the market in 50 years and reports of resistant strains emerging in less

than a decade, novel treatment strategies are needed [5, 6]. A possible solution is host-directed therapies as a potential treatment or adjuvant to shorten antibiotic regimens.

II. Infection

Tuberculosis is contracted by inhalation of *M. tuberculosis* through aerosolized droplets from close contact with an infected individual. In most cases, an appropriate immune response is sufficient to prevent active disease; however, reinfection and complete clearance of the bacteria is commonly not achieved [7, 8]. Upon *M. tuberculosis* survival, the alveolar

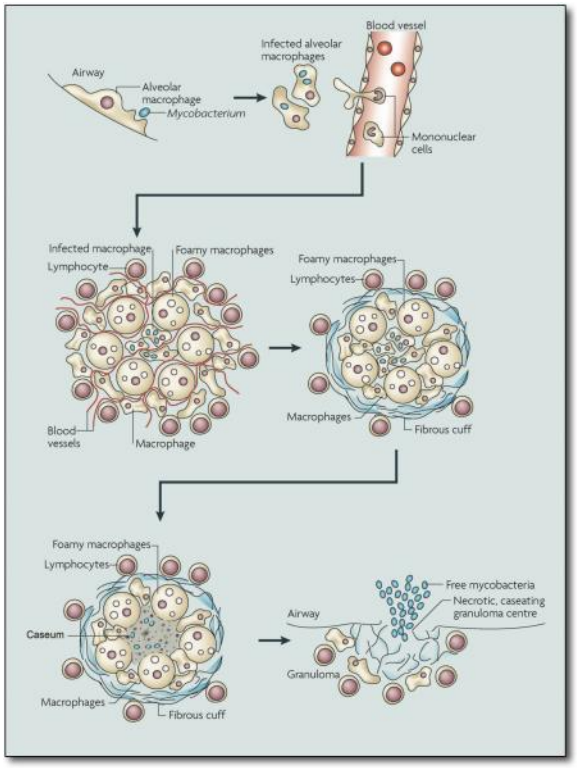

Figure 1.2. Progression of Tuberculosis Science. 2010 May 14;328(5980):852-6. doi: 10.1126/science.1184784. [9]

macrophage provides an intracellular niche for bacterial replication as immune cell infiltration begins [7, 10]. A granulomatous lesion forms from recruited mononuclear cells as the disease progresses. A mature fibrotic granuloma of macrophages, lymphocytes, and other leukocytes balances the immune response and bacterial replication [7, 11, 12]. During active disease, tissue necrosis leads to bacteria outgrowth and granuloma disruption, followed by the release of bacteria into the airway, peripheral organ dissemination, clinical symptoms, and transmission to a new host. These stages of infection can last for years with little to no clinical signs [7, 10-13].

III. Macrophage

The macrophage is a heterogeneous population of immune cells aptly named for its phagocytic activity. It is classified by lineage and phenotype, the first being bone marrow-derived or tissue-resident origins [14]. The latter develops from embryonic precursors before birth and resides in specific tissues: the lung, spleen, skin, and liver, to name a few. Resident macrophages are self-replicating and maintain a steady-state independent of the bone marrow-derived lineage [15]. Tissue-resident alveolar macrophages are one of the first cells to encounter infectious particles. Upon phagocytosis mediated by TLR4, *M. tuberculosis* employs several mechanisms to evade killing [16]. The glycosylated lipid LAM in the capsule prevents phagolysosome formation and stimulates the mannose receptor, promoting anti-inflammatory cytokines, preventing bactericidal activity, and escaping death [17, 18]. ESAT-6 mediates translocation from the phagosome to the cytosol, and once in the cytosol, there is reduced autophagy [19].

Macrophages are unique in providing a niche for *M. tuberculosis* survival, simultaneously contributing to bacterial clearance. Moreover, *M. tuberculosis* actively mediates macrophage survival, and within the alveolar macrophage, it is allowed to proliferate; however, as the disease progresses, bone marrow monocyte-derived macrophages are recruited to the sites of infection. Bone marrow monocyte-derived macrophages are more effective in killing *M. tuberculosis* than their alveolar relatives [20]. An additional difference between lineages within the lung during infection is their metabolism, and further convolution is differences in macrophage activation and function phenotypes, defined as macrophage polarization.

i. Polarization

Macrophage activation falls into classical and alternative based on exterior stimuli. *In vitro* classical activation with lipopolysaccharide and interferon-gamma results in an M1 phenotype. M1 macrophages are characterized by their pro-inflammatory phenotype with the production of TNF-α, IL-12, and IL-15. Additionally, they have been shown to upregulate iNOS, a key to antibacterial activity. Conversely, alternative activation with IL-4 produces an M2 anti-inflammatory phenotype. They are defined by their production of IL-10 and induction of arginase [21].

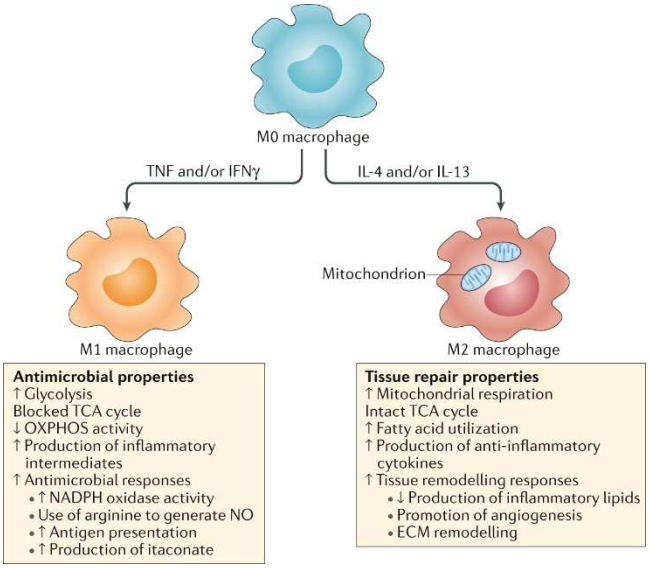

Figure 1.3. Characterization of macrophage polarization Nat Rev Immunol . 2019 May;19(5):291-304. doi: 10.1038/s41577-019-0124-9. [22]

IV. Metabolism

Metabolic pathways are responsible for energy generation, macromolecule anabolism, cellular signaling, and cell survival and death. The primary fuel for all mammalian cells is glucose. There are two main pathways of adenosine triphosphate (ATP) generation, the key molecule for energy: glycolysis and oxidative phosphorylation.

ATP is the most common energy source and, under standard conditions, is generated by two main pathways. Glycolysis is the catabolism of glucose to produce two ATP and one pyruvate molecule. Pyruvate is further metabolized, following transport to the mitochondria, to carbon dioxide by the tricarboxylic acid cycle, which drives oxidative phosphorylation and the proton gradient generation. This gradient drives ATP synthase and converts ADP to ATP. A single glucose molecule produces 34 ATP molecules during oxidative phosphorylation. Alternatives to glucose from β-oxidation, amino acid catabolism, and tricarboxylic acid cycle intermediates can fuel oxidative phosphorylation to generate ATP. Oxygen is necessary for these processes. Here select metabolic pathways are discussed as related to *M. tuberculosis* infection [23].

i. Aerobic glycolysis

Aerobic glycolysis is the conversion of glucose to lactate in the presence of oxygen. In the 1920s, Otto Warburg first observed this phenomenon in tumor cells, now called the Warburg effect [24]. This conversion was well established and contrary to conventions, where this occurs under

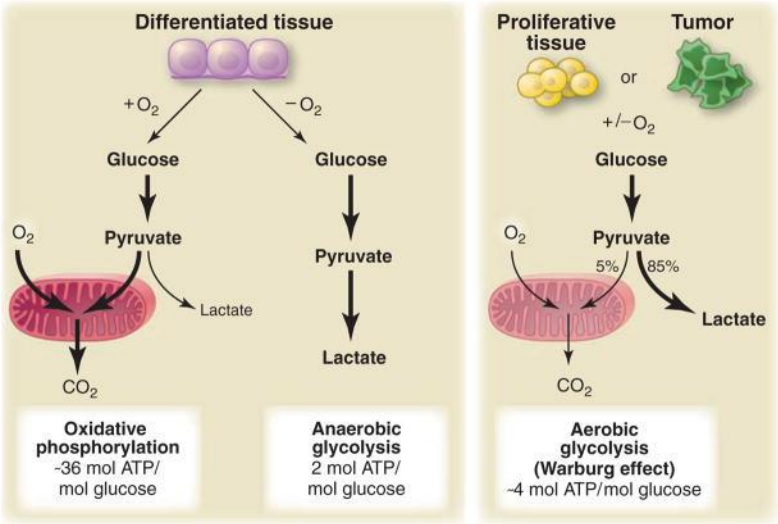

Figure 1.4. Glucose utilization under physiological oxygen conditions Science. 2009 May 22; 324(5930): 1029–1033.doi: 10.1126/science.1160809. [25]

aerobic conditions and is aptly defined as aerobic glycolysis. This metabolic shift has since been found outside of malignant cells and is a chosen mechanism of immune cells beyond proliferation [23, 26]. Aerobic glycolysis is inefficient, with eight times fewer ATP molecules generated; however, there are advantages. Modulation of metabolism allows for increased cell signaling and longevity. Aerobic glycolysis rapidly produces ATP; moreover, with the tricarboxylic acid cycle uncoupled from energy generation, intermediates may be utilized for macromolecule biosynthesis. Additionally, tricarboxylic acid cycle intermediates are critical in cell signaling and antimicrobial activity [23, 24, 26].

ii. Tricarboxylic acid cycle

The tricarboxylic acid cycle is housed within the mitochondria and comprises a series of reactions that generate ions to drive ATP production in the presence of oxygen [27]. However, these processes are not limited to energy generation. Intermediates: citrate, oxaloacetate, α-ketoglutarate, and succinyl-CoA of the tricarboxylic acid cycle are utilized for fatty, amino, and nucleic acid creation. Moreover, recent work has illuminated the contributions of the intermediates to cell signaling and bactericidal activity: acetyl-CoA, citrate, succinate, and fumarate [27].

Histone acetylation is an epigenetic modification that occurs to control gene function. Pyruvate to acetyl-CoA is the first step in the tricarboxylic acid cycle. Acetyl-CoA is a source of acetylation for posttranslational protein modifications. Elevated acetylation is associated with a proliferative cell state. Additionally, fatty acid synthesis is inhibited within activated macrophages via acetyl-CoA carboxylase

and increasing acetyl-CoA, which is converted to citrate to produce nitric oxide, a critical antimicrobial compound [28, 29].

Succinate is recognized as a vital signaling metabolite. A high level of succinate is linked to DNA and histone hypermethylation, promoting global transcriptional changes [30]. At the protein level, pro-inflammatory cytokine IL-1β is linked to succinate oxidation [31]. The accumulation of succinate within the cytosol stabilizes transcription factor HIF-1α, which increases IL-1β in activated macrophages. Additionally, the electron transport chain oxidizes succinate by complex II, succinate dehydrogenase,

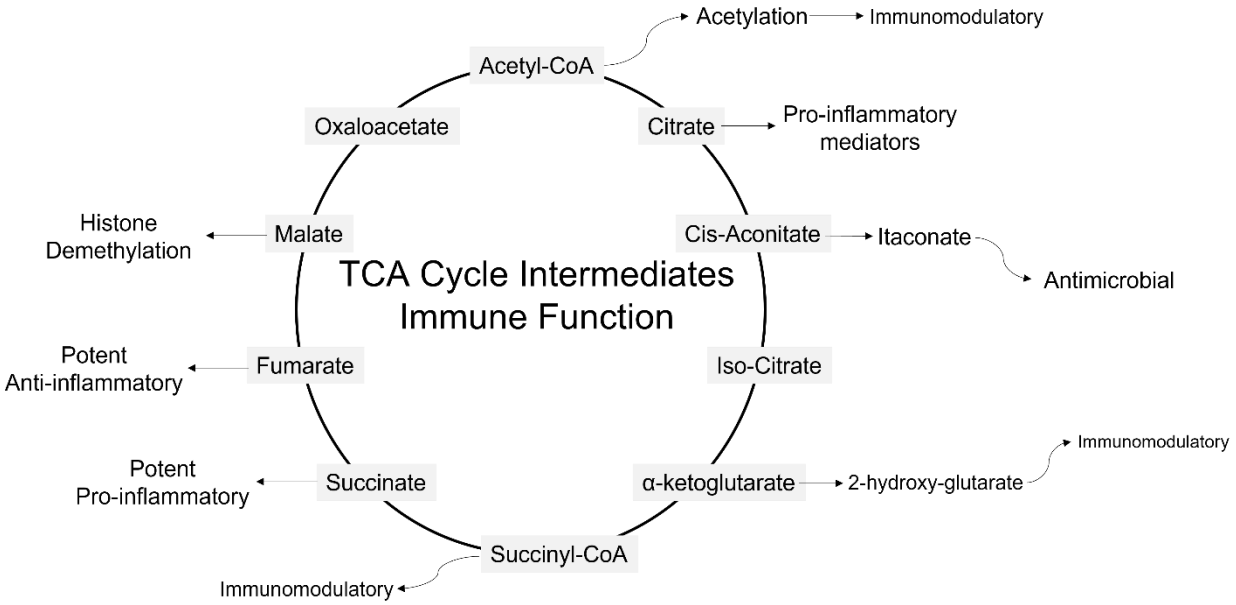

Figure 1.5. Immune function of Citric Acid intermediates Adapted from Choi et. al. PLoS Pathog. 2021 Sep; 17(9): e1009941. doi: 10.1371/journal.ppat.1009941.; Life (Basel). 2021 Jan 19;11(1):69. doi: 10.3390/life11010069.; J Leukoc Biol. 2019 Jul;106(1):105-117. doi: 10.1002/JLB.3MIR1118-415R. [32-34]

bypassing complex I. Increased ions through complex II allow the reverse electron flow back thru complex I to generate ROS for cell signaling and bactericidal nitrite oxide generation [35].

Fumarate has surfaced with its ability to induce epigenetic changes and its role in monocytes' trained immunity (innate cell memory). Fumarate accumulation increases pro-inflammatory cytokines upon restimulation, reversible with the inhibition of glycolysis and glutaminolysis. Moreover, fumarate stabilizes HIF-1α by inhibiting hydroxylation of prolyl hydroxylase domain-2 promoting pseudohypoxia [35, 36].

There is increased interest in itaconate derived from cis-aconitate produced through citrate dehydration within the tricarboxylic acid cycle in response to *M. tuberculosis* infection. The immune

responsive gene 1 enzyme catalyzes this reaction during pro-inflammatory conditions within macrophages [37]. Elevated levels of itaconic acid have been found in the lung and spleen during *Salmonella typhimurium* and *M. tuberculosis* infections. Itaconic acid's role is twofold, antimicrobial and signaling. Itaconate inhibits *M. tuberculosis* isocitrate lyase, a key enzyme in the glyoxylate shunt. This alternative pathway is upregulated during hypoxia and with alternative carbon sources to the tricarboxylic acid cycle [38].

Moreover, itaconate regulates the production of reactive oxygen species by having antimicrobial and cell signaling activities. This upregulation of reactive oxygen species by itaconate increased tumor necrosis factor alpha-induced protein 3, thereby suppressing the NF-κB signaling pathway and demonstrating anti-inflammatory pressure. The addition of an antioxidant reversed this effect [35].

V. Cell Death

Disposing of damaged, harmful, or senescent cells are essential to multicellular organisms. Just as life, death is a tightly regulated cellular process. A cascade of protein modifications triggers the cell's death, whether neoplastic or pathogen-infected. There are currently 12 classifications of programmed cell death and one non [39-41]. Here are three motifs and *M. tuberculosis* impact.

i. Apoptosis

First described in the 1800s, but not until the 1970s, was the programmed cell death mechanism of apoptosis studied in depth. Two converging pathways lead to similar morphological changes within the cell membrane and nuclei, ultimately leading to the cell's death [42]. Similar to both pathways are effector and executioner caspase proteins, seven of which are linked to apoptosis. All caspases share an aspartate-specific cysteine protease and reside as zymogens with a conserved active site between members. Upon cleavage into subunits, a heterotetramer forms the active enzyme [43-45].

Starvation, reactive oxygen species, and intracellular stress initiate the intrinsic apoptosis pathway through the posttranslational modification of the cytosolic proteins in the Bcl-2 family. The BH3 domain inhibits mitochondrial stabilizing factors and directly activates Bak and Bax, pro-apoptotic effectors within this family of proteins, oligomerization initiating mitochondrial outer membrane permeabilization [44, 46]. Within the mitochondrial inner membrane, weakly electrostatic attached

cytochrome c releases through the Bax/Bak pore to the cytosol generating the apoptosome, which requires ATP for allosteric oligomerization of seven apoptosis-protease activating factor 1 molecules [44]. The apoptosome then activates caspase-9, which remodels the mitochondria causing eventual cell death while cleaving the more efficient killer caspase-3. Prior to caspase-3 activation, cell death is inevitable; however, caspase-3 is responsible for the classic apoptosis chromatin condensation and DNA fragmentation through its protease activity [45, 47, 48].

As the nomenclature suggests, the extrinsic apoptosis pathway is initiated by a receptor-mediated interaction with the tumor necrosis factor receptor family of membrane-bound proteins. This receptor family has a cytoplasmic 80 amino acid sequence known as the death domain. Upon ligand binding, adapter proteins FAS-associated death domain protein or tumor necrosis factor receptor type 1-associated death domain protein is recruited [44]. Auto-activation of caspase-8 and 10 occurs through the death-inducing signaling complex comprised of the receptor, adapter, and caspase proteins. Further propagation of the cascade is by proteolysis of caspase-3, 6, and 7 by caspase-8 and 10. Alternatively, the cleavage of the BH3 domain by caspase-8 on Bid continues down the intrinsic pathway depending on cell lineage [45, 47].

Figure 1.6. Summary characteristics of cell death mechanisms JCI Insight. 2019 Aug 8;4(15):e128834. doi: 10.1172/jci.insight.128834.; News Physiol Sci. 2004 Jun;19:124-8. doi: 10.1152/nips.01519.2004.; Nat Rev Microbiol. 2009 Feb;7(2):99-109. doi: 10.1038/nrmicro2070. [49-51]

ii. Pyroptosis

The body of knowledge is young compared to other programmed cell death mechanisms; however, the role of pyroptosis is no less impactful. Critical features of pyroptosis are a pro-inflammatory phenotype and lytic death [49]. Morphological cells undergo rapid swelling and osmotic lysis. DAMPs or PAMPs initiate the pathway cascade through the inflammasome protein complex. The inflammasome comprises at least a nucleotide-binding oligomerization domain-like receptors and apoptosis-associated speck-like protein containing CARD, cleaving pro-caspase-1 to its active form. Caspase-1's role is two-fold. Caspase-1 mediates the N-terminal functional domain of gasdermin D generating the membrane pore allowing the release of the active form of IL-1β and IL-18 cleaved by caspase-1 [40, 52]. The efflux of potassium rapidly increases the osmotic pressure within the cell, causing swelling and lytic cell death. Caspase-3, 8, and 9 can also activate gasdermins leading to pyroptosis under typical apoptotic initiation; however, this has only been found in cells expressing high levels of gasdermins [53].

iii. Necrosis

Historically necrosis, a term used by pathologists to describe the presence of dead cells and tissue, is an unregulated form of cell death. This sudden death and release of cellular contents are pro-inflammatory and occur by physical or chemical disruption of the plasma membrane, for example; however, the term necrosis or the observation of dead cells lacks the nuance in the complexity of cell death and is just a descriptive term for the end state of multiple cell death mechanisms. Recent work has increased the body of knowledge and demonstrated unique pathways resembling the pathophysiology of necrosis [43, 54].

Necroptosis is a programmed cell death initiated by typical death receptors; FAS, TNF, and TRAIL, or intrinsic stimulation of ROS. These signals are involved in the extrinsic apoptotic pathway; however, the inhibition of caspase 8 leads to necrotic cell death through receptor-interacting serine/threonine kinase1/3 (RIPK1/3) necrosome [55]. The necrosome phosphorylates mixed lineage kinase domain like pseudokinase (MLKL) facilitating oligomerization which functions in two ways. First, actin filaments traffic oligomers from the Golgi to the plasma membrane leading to pore formation and cell rupture. Alternatively, glycosphingolipids and protein receptors in the plasma membrane generate a lipid raft of MLKL oligomers, causing an influx of sodium ions, cell swelling, and rupture [56, 57].

Either mechanism generates a pro-inflammatory environment through the release of DAMPs. Additionally, RIPK3 activates the inflammasome seen during pyroptosis, generating IL-1β and released during cell rupture. The interaction of RIPK1 and tumor necrosis factor-alpha produces additional inflammatory cytokines with the activation of NF-κB [40].

iv. *Mycobacterium tuberculosis* vs. Host

Canon dictates the simple concept that apoptosis benefits the host, whereas necrosis favors the bacteria. This statement is not without contradiction and is more complex than it appears. Macrophage studies have demonstrated that apoptosis has little to no direct bactericidal effect [13, 58]. However, a series of experiments reveal indirect antimicrobial effects. Efferocytosis, the uptake of apoptotic bodies by macrophages, neutrophils, or both, kills the bacteria by ROS and maturation of the phagolysosome. The apoptotic vesicles act as a second membrane that prevents sulfolipid and phosphatidylinositol mannoside 6 in the bacterial cell wall from preventing phagosome-lysosome fusion and bacterial effect [59]. Additional evidence of the importance of apoptosis is the work in transgenic C3HeB/Fe mice. These mice are highly susceptible to *M. tuberculosis*. A congenic strain was constructed with an active intracellular pathogen resistance 1 gene. Macrophages from the congenic strain could limit bacteria replication and underwent greater levels of apoptosis. *In vivo*, there was increased apoptosis within the granulomas compared to C3HeB/Fe mice, with improved survival rates and lower organ bacterial burden [60]. *Alox5*$^{-/-}$ mice also confer a more protective phenotype. Infected macrophages with a defective 5-lipoxygenase gene undergo apoptosis as opposed to necrosis [61]. Additional support for the importance of apoptosis is that *M. tuberculosis* actively prevents it.

M. tuberculosis has numerous ways to evade apoptosis. One is the up-regulation of Mcl-1, a prosurvival antiapoptotic member of the Bcl-2 family, found only with virulent strain infections *in vitro* [62]. Additionally, virulent bacteria inactivate tumor necrosis factor-alpha by inducing tumor necrosis factor receptor 2 secretion and preventing the extrinsic apoptosis pathway in human alveolar macrophages [63]. Through gain of function, it was shown that the *M. tuberculosis nuoG* gene, encoding a type I NADH-dehydrogenase, reduced apoptosis 8-fold in *M. kansasii*, a non-virulent mycobacterium, in human macrophages. *In vivo*, *M. tuberculosis* Δ *nuoG* mutant increased survival in immunodeficiency and

competent mouse models compared to the parent and complemented bacilli [59]. The active prevention of apoptosis is telling of its importance.

VI. Small Animal Models

Since the discovery of *M. tuberculosis*, animal models have been essential to understanding human disease. These models have informed us about pathogenesis, immune response, and viable treatments [64]. Here are discussed the central advantages and disadvantages of the two commonly used small animal models; mouse and guinea pig.

Model	Histopathology			Relative susceptibility to *M. tuberculosis*	Immunologic reagents available	Laboratory space requeriments and costs	Approximates human latent TB infection	Most common experimental uses
	Necrosis	Caseation	Cavitation					
Mouse	Variable	Usually not	No	Low	Extensive	Relative small	No; Cornell model may do so	Immunology; drug efficacy
Rabbit	Yes	Yes	Yes	Very low (*M. bovis* typically used)	Moderate	Relative large	No	Pathogenesis
Guinea Pig	Yes	Yes	Infrequent	Very high	Relatively few	Moderate	No	Vaccine efficacy; airborne transmission
Nonhuman primate	Yes	Yes	Yes	High	Extensive	Large	Yes	Pathogenesis; Immunodeficiency

Figure 1.7. Features of the mammalian animal models of tuberculosis Am J Respir Cell Mol Biol. 2008 Nov;39(5):503-8. doi: 10.1165/rcmb.2008-0154TR. [65]

i. Mouse Model

Much of our knowledge of tuberculosis is due to the mouse model. Its most significant advantage is the availability of resources, and the advent of transgenetic and knockout stains illuminated vital aspects of the immune response to *M. tuberculosis*. Within innate immunity, tumor cell lines revealed the activation of Toll-like receptors 2, 4, and 9 as protective [16, 66]. Further studies in mouse triple TLR2/4/9$^{-/-}$ and MyD88$^{-/-}$ clarified that MyD88, not TLR2/4/9, conferred protection. Moreover, differences in reports concerning the protective nature of the various TLR2/4/9$^{-/-}$ single or double mouse knockouts may be due to differences in methods [65]. Others utilizing mouse knockout demonstrated the importance of IFN-gamma, GM-CSF, and TNF-alpha. Infected mice lacking these cytokines lead to rapid disease progression and death [67]. The mouse models additionally advanced the understanding of the adaptive immune response to *M. tuberculosis*.

Studies in the mouse model have shown the importance of T cell subsets. In the early days, work was done on the delayed onset of a particular arm of the adaptive immune response, coined "delayed-type hypersensitivity." [65] Latter work in the model confirmed the protective role in the divergent differentiation of T-cells between the Th1-Th2 response [65, 67]. Furthermore, it has described the

turbulent role of regulatory T cells early in disease progression and the necessity to control the exuberant inflammatory response during the chronic stage of infection. The contributions to the field are not limited to knockout mice models [68].

Susceptibility to *M. tuberculosis* infection varies between inbred mouse strains. Genetic studies have identified the *sst1* gene locus, which affects vulnerability to progressive disease in mice. Additionally, the mouse model has been used extensively for drug and vaccine testing. Noteworthy is the fact that mice are easy to house with lower costs and have a plethora of immunological reagents [65, 67]. Despite all the advantages of the mouse model, there are drawbacks.

Mice and humans diverged some 80 million years ago, and tuberculosis has coevolved with humans. A key difference between mouse and human disease is the granuloma. Mouse lesions are more diffuse and composed of greater numbers of neutrophils. There is a lack of a true granuloma. This fundamental difference also leads to a difference in the microenvironment, which lacks necrosis and hypoxic regions. The necrotic region is significant, where large numbers of extracellular bacteria are harbored [67]. Additionally, mature fibrotic granulomas are a barrier to drug penetration.

A fundamental difference between human and mice are also present within metabolic pathways. Mice can produce vitamin C, whereas humans require it from their diet. Vitamin C plays a vital role in T- and B-cell proliferation and in phagocytes ROS production, bacterial killing, and cell death. Regions where tuberculosis is endemic converge with vitamin C deficient populations [69].

ii. Guinea Pig Model

The guinea pig was the original model where Koch proved *M. tuberculosis* as the causal agent of tuberculosis and has reemerged for vaccine and drug efficiency trials [64, 67, 70, 71]. The model's key advantage is the similarities to human physiology, progression of the disease, and pathology. Guinea pig vitamin C and fatty acid synthesis are more similar to humans than other models. The immune system of guinea pigs also shares more similarities to humans than other models. Malnutrition and micronutrients were studied in the past and are again given new tools to investigate human disease [68, 69, 72, 73].

An example is the CD1 molecule similar to major histocompatibility complex I in the presentation of lipid antigens. All mammals encode the CD1 molecule, and humans retain five isoforms;

however, mice lack four, A, B, C, and E. The advantage of the guinea pig is that it has retained these isoforms, and studies have identified intercellular localization comparable to human cellular distribution. With *M. tuberculosis* encoding over 250 genes for lipid metabolism, it is understood why CD1 is of interest [16, 74, 75].

The guinea pig is considered a susceptible model; the convention is aerosol infection with approximately 20 - 50 bacilli; however, as few as five bacteria have been shown to overtake eighty percent of animals [67, 70]. In contrast to the mouse model, inbred mouse models require 2 – 5 times as much bacteria to cause consistent disease. There is a current interest in lower initial bacterial inoculation thought better to mimic human infection in both models [76]. Studies in South Africa utilizing circulating air from human tuberculosis patients demonstrated that the guinea pigs were exposed to *M. tuberculosis*; however able to clear the bacteria, which is dogmatic that only 5 - 10% of human infection result in active disease [77, 78].

The granuloma structure in the guinea pig model resembles human disease. The granulomas form central necrosis ringed by macrophages and lymphocytes encased with fibrin, a true granuloma [67, 70]. The stark difference from human disease is that cavitation rarely occurs. Lacking cavitation results in the inability to disseminate bacteria to others, and the guinea pig model fails in studying transmission. Like humans, bacterial replication within the lung achieves a steady state, leading to a phase of infection without clinical manifestation, be it a much shorter time than humans. After this lag phase, the disease eventually overcomes the animals [67, 70]. Given these similarities to human disease, there remains a massive gap in the model's advantages compared to others. This gap is the lack of immunological reagents and genomic tools and cannot be understated. Regardless of the drawbacks, the guinea pig model has illuminated the host-pathogen interaction and is more predictive of vaccine and drug efficacy [67, 70].

VII. Therapeutics

There is a long history of interventions for tuberculosis. Currently, there is only a single approved vaccine for prevention that confers partial protection against the most severe forms of tuberculosis in children, and protection wanes by adulthood [67, 70, 79, 80]. However, numerous candidates exist in clinical and pre-clinical trials [81]. With that said, the focus here is on treatment. The current treatment

regimen for drug-sensitive strains is a four-drug cocktail for 6-8 months under direct observation. For multi-drug resistant tuberculosis, the treatment is five antibiotics for 20 months of second-line drugs, which have increased side effects. Extensively drug-resistant tuberculosis has little consensus for treatment and depends significantly on drug susceptibly testing. The treatment landscape is ever-changing, with the WHO issuing a new recommendation as recently as March 2022 [82].

Before the discovery of antimicrobials, treatment for tuberculosis consisted of supportive care, a healthy diet, clean air, and surgical techniques. These surgical interventions were invasive and failed to purge the bacteria completely [83, 84]. Nearly twenty years after the discovery of penicillin, streptomycin was the first antibiotic found to be effective in treating *M. tuberculosis* in the guinea pig model. In the late 1940s, human trials in the United Kingdom definitely confirmed streptomycin's efficacy against pulmonary disease, a higher burden of proof than miliary tuberculosis, with mortality near 100% without treatment [85]. This striking discovery was not without reservation and found that a fifth of patient infections were resistant to streptomycin within four months of the end of treatment. Furthermore, over half of the patients reported severe side effects [3, 83-85].

Over the next twenty years, there was extensive research into tuberculosis drug discovery with breakthroughs of new chemotherapies and antibiotics. The flurry of research and public health measures ended abruptly in the late 1960s when rifampin became the bedrock of the three-drug therapy with isoniazid and ethambutol [84]. With a tool to defeat the disease, attention to tuberculosis faltered. It was

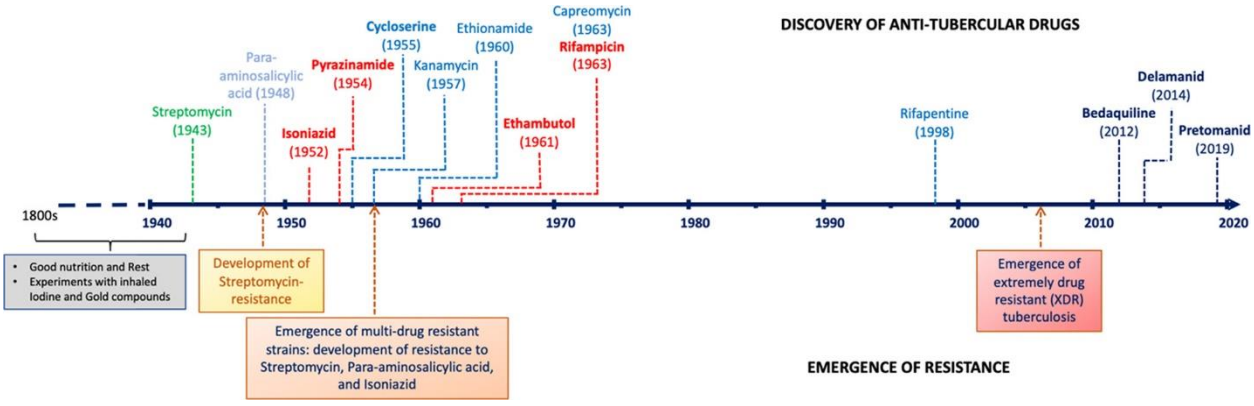

Figure 1.8. Timeline of tuberculosis treatment Acc Chem Res. 2021 May 18;54(10):2361-2376. doi: 10.1021/acs.accounts.0c00878. [86]

not until the emergence of the HIV epidemic in the 1980s did the world become aware of the growing tuberculosis problem. In seven years, cases increased by 20% in the United States, and once again, drug

resistance, this time to rifampicin and isoniazid, returned from the past; but a renewed effort to eradicate the disease did also [3, 4, 83].

Since then, drugs, fluoroquinolones and linezolid, have been repurposed against *M. tuberculosis*. Even clofazimine, once relegated to fight leprosy, has increased interest in multidrug-resistant infections. Moreover, after 40 years, a new drug was approved by the US Food and Drug Administration, and since 2012 two more in the fight against drug-resistance tuberculosis [5]. Lessons from the past teach that compliance is a pitfall, and new therapeutic strategies are still needed.

i. Host-directed therapy

It is established that no single treatment will eradicate tuberculosis, and a diverse treatment strategy is required because a single antibiotic treatment leads to resistance. Bedaquline, approved by the US Food and Drug Administration in 2012, took less than five years for resistant strains to emerge, and antibiotic resistance has been recognized since its use in tuberculosis treatment [6]. Host-directed therapies are not new in tuberculosis, but they have expanded their scope of function to treat the disease. These therapies aim to tailor the immune response to optimize antimicrobial activity and suppress damaging inflammation. One of the first treatments was corticosteroids for their anti-inflammatory and immunosuppressive properties, which are still used today in tuberculous meningitis, the most lethal form of tuberculosis [79, 87]. Here is discussed the antiglycemic drug metformin.

Metformin, the biguanide drug class, is one of the most commonly prescribed drugs globally and has an extensive safety profile. It has unique properties which target the damaging effect of an *M. tuberculosis* infection. *M. tuberculosis* infection has been shown to disrupt glucose homeostasis in the guinea pig model and is treated aggressively in humans with diabetes mellitus comorbidity [88-92]. The bacteria do not directly cause damage to the lung, where an overexuberant immune response and oxidative stress are interconnected, leading to necrosis and cavitation. Metformin has antioxidant and anti-inflammatory properties by reducing tumor necrosis factor alpha and interleukin 1 beta; furthermore, it upregulates nuclear factor erythroid 2-related factor and glutathione [89]. Metformin is a partial mitochondrial complex I inhibitor that reduces ROS production and is utilized for cell signaling and activation to reduce the immune response further. Additionally, metformin activates adenosine monophosphate-activated protein kinase phosphorylating p53 and peroxisome proliferator-activated

receptor gamma coactivator 1-alpha, to name two, inhibiting nuclear factor kappa-light-chain-enhancer of activated B cells [88].

Metformin is proving itself as an adjunctive therapy in animal models and the clinical realm. In the mouse and guinea pig models, metformin was found to increase $CD4^+$ and $CD8^+$ T-cells, and reduce bacterial and lesion burden during the chronic stage of infection. There is a marked reduction in sputum culture conversion time in humans, which is critical to clinicians as a leading indicator of treatment efficacy and reduced morbidity in diabetic and non-diabetic patients [88, 90, 92]. Metformin, taken together, is a candidate as a host-directed therapy; however, more research is needed into the mechanism of action, which may lead to increased therapeutic targets.

HYPOTHESIS AND SPECIFIC AIMS

Hypothesis

Metabolic inhibitors, metformin and 2-deoxy-glucose, utilized in combination during *in vitro* and *in vivo* *Mycobacterium tuberculosis* infection, restores mitochondrial stability and promote antimicrobial activity.

This hypothesis will be tested with the following aims:

Aim 1

Establish the efficiency of metformin and 2-deoxy-glucose in promoting the antimicrobial activity of macrophages.

Aim2

Evaluate the metabolic effect of *Mycobacterium tuberculosis* infection on macrophages.

Aim3

Determine the viability of metformin and 2-deoxy-glucose as a host-directed therapy in the guinea pig model of *Mycobacterium tuberculosis* infection.

MATERIALS AND METHODS

Mycobacterium tuberculosis

For *in vivo* and *in vitro* experiments, *M. tuberculosis* H37Rv (TMC #102, Trudeau Institute) culture stocks were grown under aerobic conditions with agitation in a Proskauer-Beck medium (HIMedia) containing 0.05% Tween-80 (Sigma). Cultures were collected at OD600nm between 0.8 to 1.0 and frozen at -80°C in glass vials. Serial dilutions determined the stock titer on Middlebrook 7H11 agar (BD Difco) supplemented with 10% OADC (VWR), 50 µg/ml of carbenicillin (Gold Biotechnology), and ten µg/ml cycloheximide (Gold Biotechnology) incubated for six to eight weeks at 37°C.

Guinea Pig Infection and Sample Collection

Four-week-old outbred female Dunkin-Hartley guinea pigs were purchased from Charles River and housed in the biosafety level 3 laboratory at Colorado State University Laboratory Animal Resources, accredited by the American Association for Accreditation of Laboratory Animal Care. Approval was obtained for animal procedures by Colorado State University Animal Care and Usage Committee in accordance with the National Research Council's Guide for the Care and Use of laboratory animals. Low-dose aerosol infection was delivered using a Madison Chamber aerosol device calibrated to deliver approximately 20 bacilli per animal in water. Animals were treated daily at specified initiation time points with 25 mg/kg of metformin (Spectrum Chemical MFG Corp), 145 mg/kg of 2-deoxy-glucose (Cayman Chemical), or in combination in a carrier suspension of 50% ORA-sweet (Perrigo) 50% water, or mock-treated with the carrier. At necropsy, guinea pigs received 50 mg/kg of ketamine and 5 mg/kg of xylazine via IM injection for anesthetic induction. Under terminal anesthesia, blood was collected, and animals were euthanized with an overdose of pentobarbital. Tissues were collected for histopathology by fixing with 4% paraformaldehyde (Electron Microscopy Sciences) or stored at -80°C for bacterial enumeration.

Histology

Representative tissue sections were evaluated at 200x magnification to estimate the area of inflammation relative to normal tissue parenchyma. Fixed tissues were paraffin-embedded, sectioned at five microns, and stained with hematoxylin and eosin. Total lung and lesion areas were quantified using Stereo Investigator area fraction fractionator software (MBF Bioscience) and the Nikon Eclipse 80i microscope. A

total of 20–25 randomly selected fields with a spacing of 200um defined areas of interest. Probes were assigned to uninvolved and lesion by counting frames within a 2000 μm2 area. Lesion burden was calculated as a ratio of the lesion to tissue area and expressed as a percentage. For staggered metformin histopathology analysis, the percent lesion to lung was normalized to the untreated group per experiment.

Bacterial Enumeration

Organs were weighed, diluted in PBS, and homogenized. As stated above, tissue homogenates were serially diluted, plated, and incubated. The tissue bacterial burden was calculated as log CFU per gram of tissue.

Guinea Pig Bone Marrow-Derived Macrophages

Bone marrow was collected from the femur of naïve animals and stored in 85% FBS (Atlas Biologicals) and 15% DMSO (Fisher) in the vapor phase of liquid nitrogen. Cells were maintained in RPMI with L-glutamine (Fisher) supplemented with 10% FBS (Atlas Biologicals), 100 units/mL of penicillin, 100 μg/mL of streptomycin (Fisher), and 250 ng/mL of Amphotericin B (Fisher) supplemented with 20 ng/mL M-CSF (Gemini Bioproducts) at 37°C with 5% CO_2 for seven days. After three days, additional M-CSF was added to the cultures. For macrophage infection with *M. tuberculosis*, cells were allowed to adhere to wells for 24 hours, infected at an MOI of 5:1, unless expressly noted in the particular section, or with bacterial stock supernatant for four hours, and washed with Hank's Balanced Salt Solution (Fisher). Cells were exposed to 25 μg/mL of gentamycin (Gold Biotechnology) for one hour to remove extracellular bacteria and triple rinsed in cell culture media. Macrophages were treated in culture media supplemented with 20 ng/mL M-CSF, 600μM metformin, 700μM 2-deoxy-glucose, or in combination and incubated at 37°C with 5% CO_2.

Metabolic Respirometry

According to the manufacturer's instructions, peripheral blood mononuclear cells were isolated from whole blood by density gradient centrifugation with Lympholyte Mammal (Cedarlane). 5 x 10^5 macrophages, infected and treated as stated above, or 4 x 10^5 PBMCs from infected animals were seeded into 96 or 24 well Seahorse cell culture microplates coated with CellTak (Corning) in Seahorse XF assay media (Agilent Technologies), respectively. Plates were centrifuged for 5 minutes at 500 x g with no brake for cell adhesion, and CO_2 was outgassed for 30 minutes at 37°C. An Agilent Seahorse XFe24

or XFe96 bioanalyzer measured oxygen consumption and extracellular acidification rates. Basal readings were taken, followed by injections of 1 μM oligomycin (Sigma-Aldrich), 1.5 μM trifluoromethoxy carbonylcyanide phenylhydrazone (Cayman Chemical), 0.5 μM rotenone and antimycin A (Sigma-Aldrich), and 50 mM 2-deoxy-glucose (Cayman Chemical). Glycolysis and mitochondrial respiratory parameters were calculated based on the manufacturer's instructions. Data were analyzed as stated in the figure legend based on the dataset.

Cell Viability

Macrophage viability with treatments and infection was assessed in a 96-well format at 7.5 x 10^5 cells per well. Cells were washed and suspended in 50 μL of Hank's Balanced Salt Solution. 5 μL of 12M MTT (Fisher) stock was added to the wells and incubated at 37°C with 5% CO_2 for four hours. 200 uL of DMSO was added to wells for 10 minutes, mixed, and read at 590nm on a Biotek Synergy 2 spectrophotometer. Live macrophages were calculated based on a standard curve. To determine the effect of infection on the viability of treated cells, data was Box-Cox transformed [93], and three-factor interaction was evaluated. P-values were adjusted with the Holm method. Analysis was performed using R version 3.6.1.

For bacterial viability, media was collected, replaced with 1% Triton-X (Sigma-Aldrich), agitated, and triple rinsed with water. As stated above, samples were plated on 7H11 agar for CFU determination. Percent viability was calculated based on the initial cells plated for macrophages and bacteria.

Mitochondrial Membrane Potential

Macrophages were plated and infected, as stated above. At specified time points, media was replaced with Hank's Balanced Salt Solution, and cells were incubated with 64nM of tetramethylrhodamine methyl ester perchlorate (Fisher) for 30 minutes at 37°C with 5% CO_2. Media was removed, and cells assayed in 50 μL of fresh Hank's Balanced Salt Solution with a Biotek Synergy 2 spectrophotometer at an excitation wavelength of 530/25nm and emission at 590/35nm. Relative fluorescent units were standardized to cell numbers with MTT assay, as stated above. Data were normalized to the maximum value determined based on each assay. The assay was performed three times with five replicates each, and replicates were removed if the cell number was below the detectable limit. One value from the uninfected 72-hour time point was removed based on Turkey's IQR outlier determination. Value was greater than 3.5 times IQR.

Malondialdehyde Quantification

Macrophages were seeded into 60 x 15 mm untreated polystyrene Petri dishes (VWR). 3 x 10^6 cells were infected and treated, as stated above. Samples were collected and assayed with a Lipid Peroxidation Colorimetric Assay (Biovision) based on the manufacturer's instructions. Protein concentrations, quantified by Pierce BCA Protein Assay (Fisher), normalized malondialdehyde concentrations. The assay was performed three times in duplicate. One value from the untreated and 2-deoxy-glucose 24-hour time point was removed based on Turkey's IQR outlier determination. Value was greater than 4.5 and 4.0 times IQR, respectively.

Flow Cytometry

Cells were infected and treated in 24-well plates. At specified time points, media was replaced and stained with FLICA 660 Caspase-1 probe (ImmunoChemistry Technologies) for 30 minutes at 37°C with 5% CO_2. The buffer was changed to an Annexin V binding buffer, 10mM HEPES, 140mM NaCl, and 2.5mM $CaCl_2$ (Sigma-Aldrich), and pH was balanced to 7.4, which was used throughout the remaining staining for all steps. Cells were stained with Annexin V, Zombie NIR (Biolegend), and fixed with 4% paraformaldehyde in Annexin V binding buffer for 15 minutes, separated by washes with Annexin V binding buffer. Single-cell suspensions were prepared by scraping the wells, and at all steps, non-adherent cells were recovered by centrifugation at 600 x g for 6 minutes. Data was collected with the Aurora Spectral Cytometer (Cytek Biosciences) and analyzed using FlowJo software (FlowJo).

Metabolic Substrate Capacity

The capacity of infected treated cells to utilize intermediate glycolytic and TCA cycle substrates was determined using the 96-well format Mitochondrial Function Assay, MitoPlate S-1 (Biolog). Briefly, 32 substrates are imprinted on a preloaded 96-well plate in triplicate and hydrated with a supplied assay mix for one hour at 37°C. Cells were treated for 24 hours, removed with Cellstriper (Corning), washed in Hank's Balanced Salt Solution, and resuspended in MAS buffer (Biolog). Fifty thousand cells were seeded per well, and 25 µg/mL of saponin (Sigma-Aldrich) was added. Plates were read with a Biotek Synergy 2 spectrophotometer at 590nm every 15 minutes for 4 hours. Analysis was conducted in R version 3.6.1. Interaction second-degree polynomial models were constructed with an interaction on the Time variable alone and with separate intercepts for each well position per plate. The data is presented

as the rate of change, which is the linear effect's coefficient centered at two hours. Confidence intervals were constructed using the standard errors for the differences as estimated by the models. Degrees of freedom were calculated with Satterthwaite's method for denominator degrees of freedom to account for the unbalanced data. P-values were adjusted within each substrate with a Bonferroni method, and adjustments were made separately for each group.

Statistical analysis

Statistical summary, n, mean, error, and statistical significance are contained within the figure. One and two-factor ANOVA was used to determine mean differences, and data were log-transformed when required. Welch's ANOVA test was used when homoscedasticity could not be achieved, and the Kruskal-Wallis test for non-parametric datasets. Post-hoc comparison methods were Tukey or Dunn multiple comparisons test, respectively. Data were analyzed with Graph Pad Prism v.8 or R. When R analysis was required, it is stated within the specific section. Tukey's IQR rule [94] was used to determine outliers within datasets and, when used, is stated within the section. A greater rigor was used, requiring a value greater than three times the IQR to be removed.

RESULTS

Metformin and 2-deoxy-glucose treatment exacerbate disease when started at the peak of the adaptive immune response in guinea pigs.

During the chronic stage of the disease, previous studies demonstrated that metformin reduced lung bacterial and lesion burden in the guinea pig model when given four weeks before infection. We hypothesized that metformin would reduce inflammation when started four weeks after low-dose aerosol infection, the peak of the adaptive immune response in guinea pigs. On day 90 post-infection, metformin significantly reduced the mean lesion burden in guinea pigs when the treatment began before infection, 65% decrease; moreover, there is a lower trend in lesion burden when the treatment begins concurrent or two weeks after infection, 62%, and 51% reduction, respectively. However, there is an 84% increase in mean lesion burden when metformin treatment begins at four weeks of infection (Fig. 2.1).

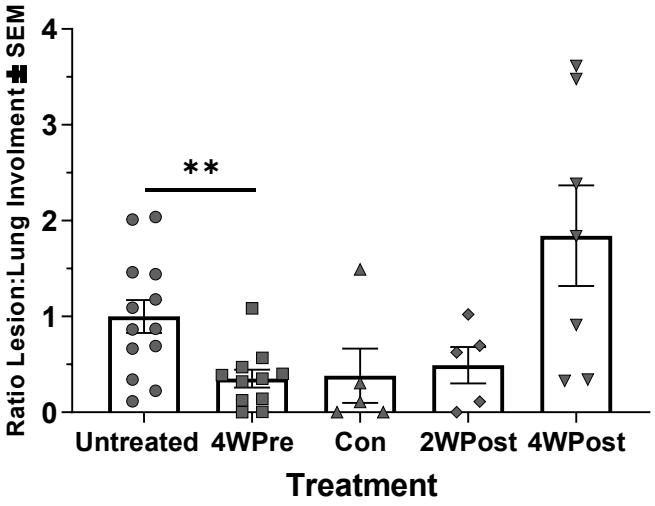

Figure 2.1. Metformin improved lung lesion burden when administered before or early during infection. Lung lesion burden at 90 days post-infection with staggered metformin administration. Metformin improves disease severity when administered prior to the onset of adaptive immunity. Duncan-Hartley guinea pigs received oral administration of 25 mg/kg metformin or carrier treatment beginning four weeks prior, concurrent, two weeks post, or four weeks post-low-dose aerosol infection with *M. tuberculosis* H37Rv. Lungs were collected 90 days post-infection, and the lesion-to-lung ratio was calculated and normalized to untreated by experiment. Welch's ANOVA test was used with Dunnett's adjustment for multiple comparisons because of the unbalanced design and lack of homoscedasticity. n = 5 – 13 animals per group; ** $p \leq 0.01$.

We tested whether inhibition of glycolysis would also reduce inflammation. On day 90 of infection, there was no significant difference in organ tissue CFU when treated with metformin, 2-deoxy-glucose, or in combination (Fig. 2.2A). However, there was a trend in a more significant lesion burden in the lung and

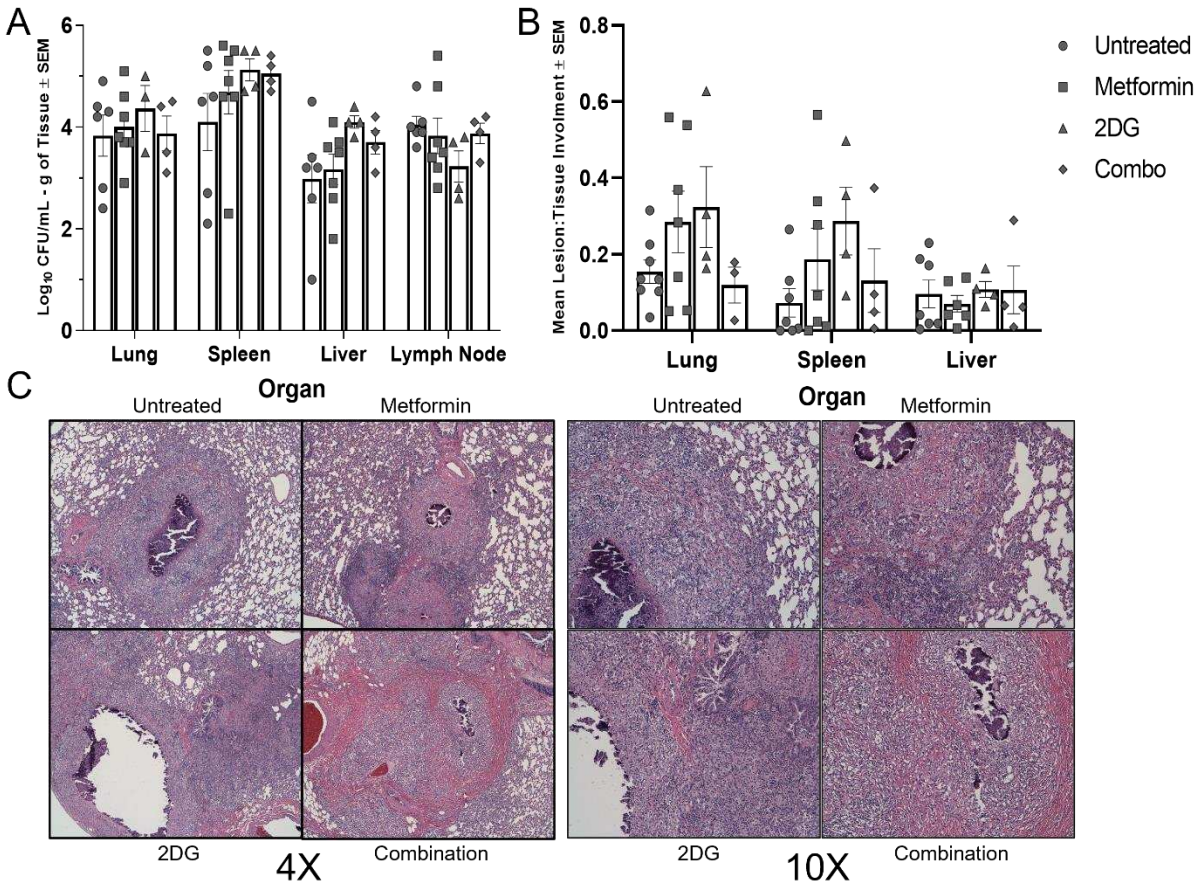

Figure 2.2. Single metabolic pathway inhibitors display increased lesion burden while combination promotes healing. A less severe lesion burden was found on day 90 of infection in combination-treated animals with signs of healing in the lung. Total lesion area burden and CFU was similar in untreated- and combination-treated animals. In metformin- and 2-deoxyglucose-treated animals, an increase in lesion-to-lung and -spleen burden; however, there was no difference in CFU (A, B). Lung, spleen, liver, and lymph nodes were collected from euthanized untreated-, metformin-, 2-deoxyglucose-, or combination-treated guinea pigs to evaluate bacterial burden (A) and lesion burden (B). Colony-forming units were generated by plating homogenized lung, spleen, liver, or lymph node tissue on 7H11 agar plates and quantified per gram of tissue (A). Stereo Investigator software was used to calculate the percent lesion to the total area in guinea pig lungs, spleens, and liver (B). Images are taken from animals that represent mean lesion burden (C). Data were analyzed by two-factor ANOVA.

spleen of metformin and 2-deoxy-glucose treated animals. Combination treatment reversed this trend in the lung, and lesion burden was similar to untreated animals (Fig. 2.2B). Lung tissue histology showed

similar granuloma morphology with single treatments to untreated. There was an increase in fibrous connective tissue organization with combination treatment, suggesting increased lesion healing (Fig. 2.2C).

A combination of metformin and 2-deoxy-glucose treatment promotes the survival of infected cells, simultaneously decreasing *M. tuberculosis* viability.

We utilized the macrophage infection model to investigate metabolic pathways' role in disease. Initially, we determined the effects of the treatments and infection on the viability of the guinea pig bone marrow-derived macrophages (GpBMMϕ) and *M. tuberculosis*. In uninfected cells, we observed an increase in cell proliferation in the untreated group; however, metformin alone inhibited this at 24 hours, and there was a significant decrease in cell viability by 72 hours of treatment (Fig. 2.3A). In contrast, 2-deoxy-glucose caused a dramatic decrease in viability at all time points. Combination treatment had an intermediate effect on viability (Fig. 2.3A).

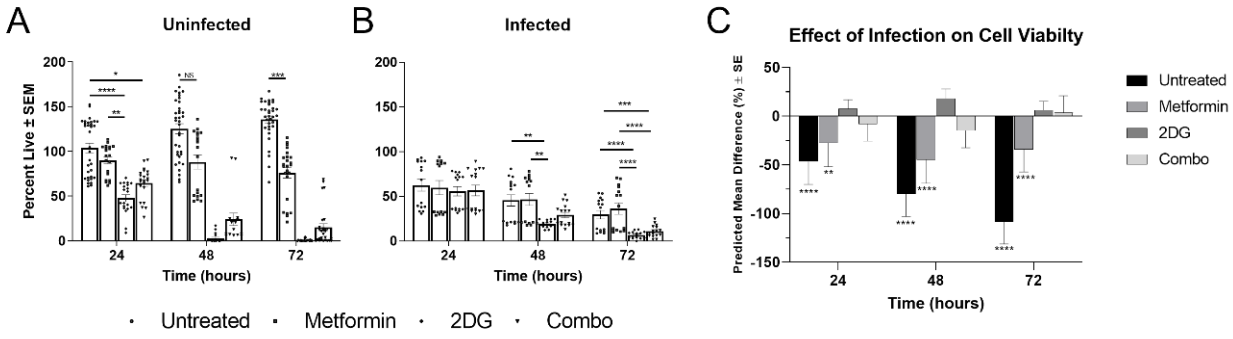

Figure 2.3. Metformin and 2-deoxy-glucose, in combination, prevent cell death due to *M. tuberculosis*. Metformin inhibits proliferation compared to untreated over the 72 hours in uninfected GpBMMϕ; additional, 2-deoxy-glucose alone or in combination with metformin was shown to be toxic (A). With infection, at an MOI of 5:1, there is no difference between untreated and metformin-treated cells. By 72 hours post-infection, 2-deoxy-glucose and combination-treatment reduced viability compared to untreated and metformin-alone treated cells (B). To determine the effect infection had on cell viability, the predicted mean difference was calculated between uninfected and infected GpBMMϕ. Untreated cells demonstrated the greatest reduction in viability. Notably, 2-deoxy-glucose and combination treatment had no additional killing or prevented toxicity during infection (C). GpBMMϕ viability was measured with MTT assay. To compare the difference in viability between uninfected and infected GpBMMϕ, data were normalized by Box-Cox transformation. A three-factor ANOVA model with three-way interaction between Time, Treatment, and infection Status was used to determine significance n = 9 – 40 (A, B). * $p \leq 0.05$, ** $p \leq 0.01$, *** $p \leq 0.001$, **** $p \leq 0.0001$.

We found no difference in cell viability between untreated and metformin-treated cells across all time points in infected cells. By 48 hours, there was a significant decrease in cell viability in 2-deoxy-glucose-treated cells compared to untreated and metformin-only treatments. At 72 hours, 2-deoxy-glucose and combination treatments had significantly lower viability than untreated and metformin

treatments (Fig. 2.3B). In determining the interaction between treatment and infection, we found untreated cells experienced the most significant loss in viability at all time points due to infection followed by metformin-only treatment (Fig. 2.3C). In contrast, in 2-deoxy-glucose treated cells, there was no additional killing due to infection. Moreover, in 2-deoxy-glucose-only treated cells at 48 hours, we observed an increase in survival compared to uninfected. The combination treatment demonstrated no additional killing due to infection (Fig. 2.3C).

We measured bacterial survival with the total CFU of intracellular and extracellular *M. tuberculosis*. Treatments did not affect bacterial survival without GpBMMϕ, and we recovered ~95% of inoculum (data not shown). Bacterial survival was similar in all treatments at 24 hours, with a modest increase in *M. tuberculosis* compared to inoculum in all treatments except for the combination treatment, where there was a significant increase. By 48 hours, we observed a trend in decreasing *M. tuberculosis* survival and a significant decrease in metformin and combination treatments (Fig. 2.4A). At 72 hours, metformin and combination treatment had significantly lower *M. tuberculosis* viability than untreated (Fig. 2.4B).

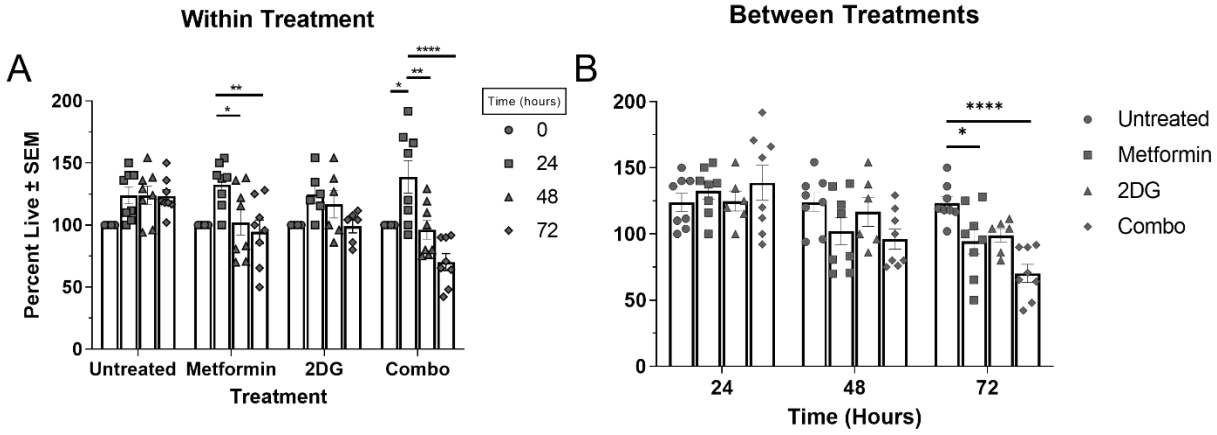

Figure 2.4. Combination treatment promotes bacterial killing in GpBMMϕ. The combination treatment significantly reduced bacteria by 72 hours post-infection compared to untreated and 24-hour peak bacterial viability. GpBMMϕ were infected at an MOI of 5:1, and bacterial viability assess at 24-hour intervals. Bacterial viability data were analyzed by two-factor ANOVA n = 8. * $p \leq 0.05$, ** $p \leq 0.01$, **** $p \leq 0.0001$.

The metabolic output of infected cells is lower during infection.

Provided that metformin and combination treatments affected bacterial clearance, we hypothesized that the infected GpBMMϕ underwent a metabolic flux. Initially, we assess the oxygen

consumption rate (OCR), a surrogate of mitochondrial respiration, and extracellular acidification rate (ECAR), a measure of glycolysis, at increasing MOI without treatments. We found that both OCR and ECAR increased. ECAR increased rapidly dose-dependently and peaked by 150 minutes. The increase in OCR was delayed compared to the ECAR and peaked at 175 minutes (Fig. 2.5A-B). These changes were short-lived, and OCR returned to uninfected levels by 300 minutes. Simultaneously, ECAR in 5:1 MOI also returned to uninfected levels, and 10:1 was decreasing by the endpoint (Fig. 2.5B).

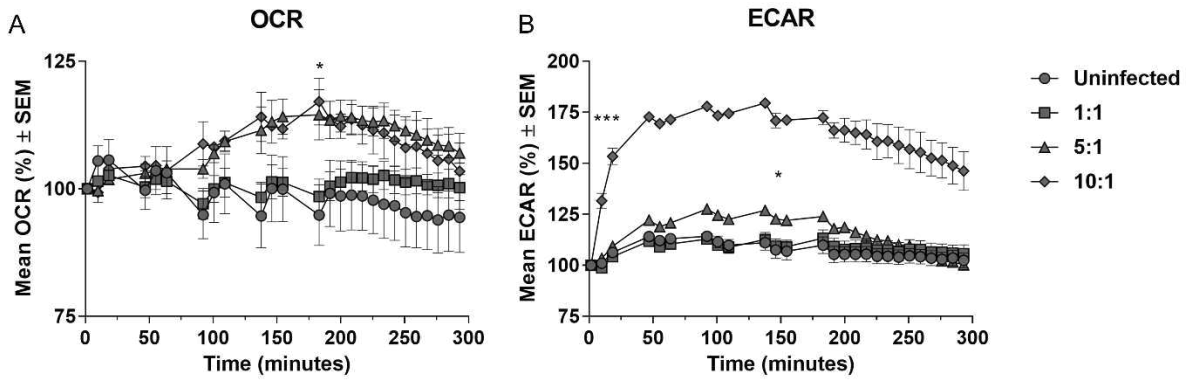

Figure 2.5. GpBMMϕ increased metabolic output to increasing bacterial load. Increased OCR was observed in the higher MOIs by 3 hours; however, upon peaking, OCR returned to uninfected levels by five hours (A). ECAR increased immediately in a dose-dependent manner. By five hours, ECAR was decreasing or returned to uninfected levels. GpBMMϕ were infected at increasing MOI, and metabolic pathways were immediately measured with an Agilent Seahorse Respirometer.Data were analyzed by two-factor ANOVA n = 3. * $p \leq 0.05$, *** $p \leq 0.001$.

After the initial experiment, cells were infected for an hour before treatment and monitored for seven hours to determine the effects of metformin and 2-deoxy-glucose on mitochondrial respiration and glycolysis. Metformin inhibits complex I of the electron transport chain, and treated cells displayed a decreasing OCR and increasing ECAR over time. Conversely, 2-deoxy-glucose treatment increased OCR and decreased ECAR. The combination treatment displayed an intermediate effect on the infected cells decreasing OCR and ECAR compared to infected cells (Fig. 2.6A-B). A complete analysis between groups is found in Supplemental T1.

At 24 hours, basal OCR was reduced in all infected groups and significantly in treated cells compared to uninfected. Metformin, 2-deoxy-glucose, and combination treatments significantly decreased OCR compared to untreated cells with combination treatment, -58.8, -64.0, and -112.8 pmol/min, respectively (Fig. 2.6C). ECAR resulted in similar trends as the seven-hour mark. There was no compensation in ECAR for the decrease in OCR in the untreated group, and there was no difference

between infected and uninfected cells without treatment. Metformin-only treated cells remained significantly elevated compared to all other groups. Conversely, in 2-deoxy-glucose and combination treatments, there was a significant reduction (Fig. 2.6D).

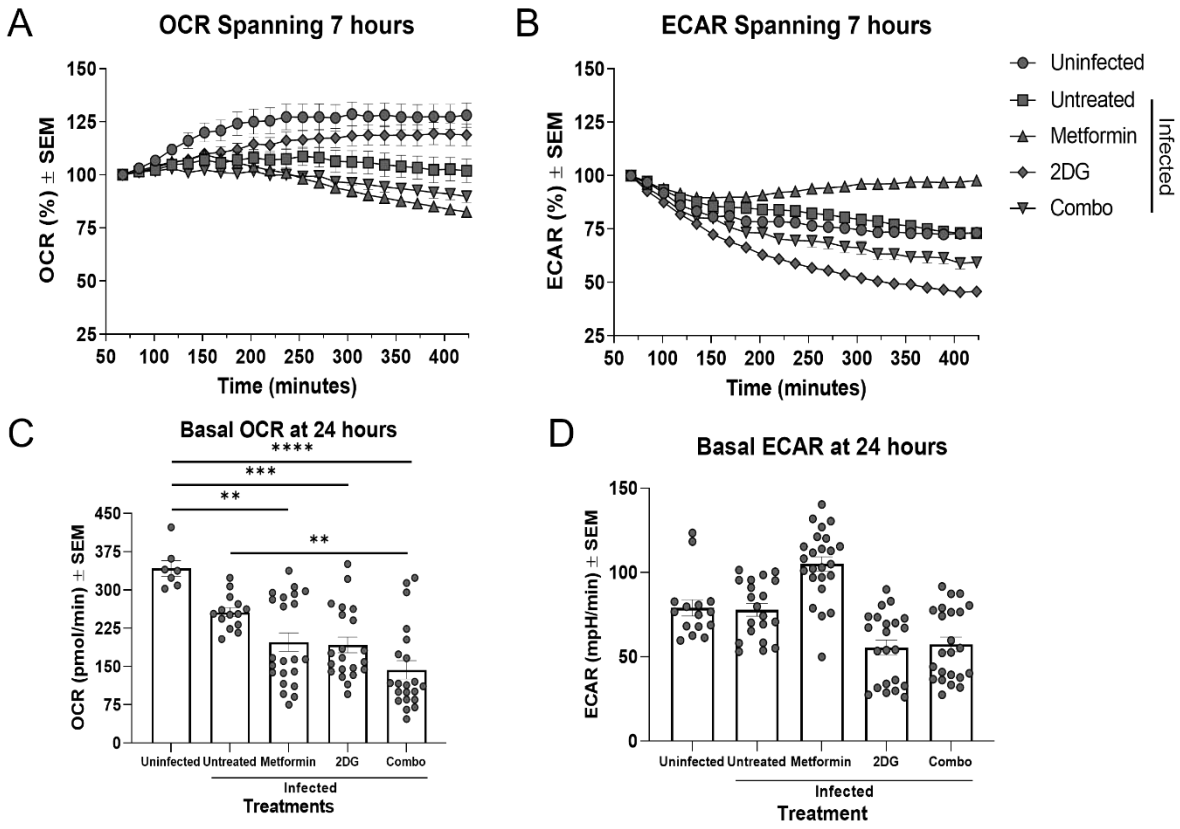

Figure 2.6. Infection reduces mitochondrial energy output with or without metformin and 2-deoxy-glucose treatment. GpBMMϕ were infected at an MOI of 5:1, allowed to rest for one hour, and metabolic pathways were measured with an Agilent Seahorse XFe96. *M. tuberculosis* infection has a greater impact on OCR than ECAR in GpBMMϕ. Early during infection, infected GpBMMϕ demonstrate a reduction in OCR; however, they show no difference in ECAR compared to uninfected control over time. In contrast, metformin reduces OCR while increasing ECAR. 2-deoxy-glucose had the opposite effect. Moreover, combination treatment reduced OCR and ECAR, not to the magnitude of single treatments (A, B). At 24 hours post-infection, OCR was lower in all infected groups than in uninfected cells. OCR was further depressed in treated cells, and 2-deoxy-glucose failed to increase OCR (C). Contrasted is ECAR maintaining trends due to infection and treatments (D). Data were normalized to starting values (A, B) or expressed as calculated raw values (C, D). Data were analyzed by a mixed-effect model with the Geisser-Greenhouse correction because of the unbalanced nature of the dataset and Tukey's multiple comparison test. A table of significance is located in supplement table 1 (Supplement T1). (A, B) n = 3 – 12; A one-factor ANOVA was used for data analysis. (C, D) n = 7 – 24; * $p \leq 0.05$, ** $p \leq 0.01$, *** $p \leq 0.001$, **** $p \leq 0.0001$.

Mitochondrial integrity improved with combination treatment.

Previous studies have shown that *M. tuberculosis* infection damages the mitochondria, and we examined differences in mitochondria respiration with our findings of a reduced OCR. There was no difference in the calculated ATP production based on OCR between infected groups (Fig. 2.7A).

However, there was elevated proton leak in the untreated group, significantly compared to 2-deoxy-glucose and combination treatments, which is associated with increased ROS levels within the mitochondria (Fig. 2.7B). However, elevated ROS can lead to oxidative damage. We measured intracellular levels of malondialdehyde at 24 and 48 hours, and it was significantly elevated in the untreated group compared to all others at both time points (Fig. 2.8B).

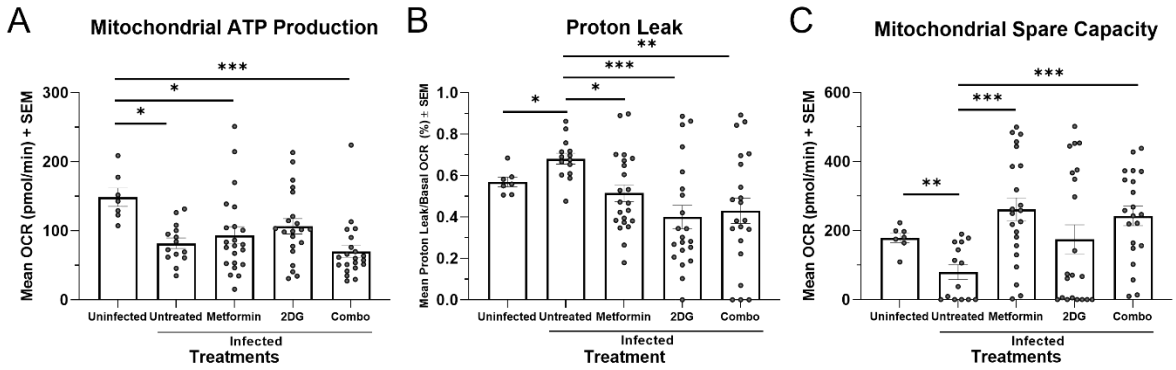

Figure 2.7. **Combination treatment prevents mitochondrial stress in infected GpBMMϕ.** Elevated OCR during infection in untreated compared to treated GpBMMϕ was not due to mitochondrial ATP production (A) but increased proton leak (B). Moreover, reduced mitochondrial spare capacity (C) with increased proton leak indicates increased mitochondrial stress. Data were calculated from 24-hour OCR measured by Agilent Seahorse XFe96. A Welch or Kruskal-Wallis one-factor ANOVA was used to determine the significance between groups with Dunnett or Dunn's multiple comparisons test, respectively. n = 15 – 24; * $p \leq 0.05$, ** $p \leq 0.01$, *** $p \leq 0.001$.

An additional measure of mitochondrial function is spare capacity, and a reduced spare capacity is associated with aging and mitochondrial damage. There was a diminished mitochondrial spare capacity in the untreated group compared to all others. In the metformin- and combination-treated groups, the spare capacity was significantly increased compared to untreated, 182.1 and 162.9 pmol/min, respectively (Fig. 2.7C). With changes in proton leak and spare capacity, we measured the mitochondrial membrane potential to examine further mitochondrial homeostasis. A rapid decrease or increase in membrane potential is associated with mitochondria dysfunction. We found elevated levels at 24 hours in all infected groups. By 48 hours, there is a collapse in the untreated and metformin-treated cells. In contrast, there is a delay in the 2-deoxy-glucose treated group, and with combination treatment, we found a stable membrane potential (Fig. 2.8A).

In the continued investigation of mitochondria respiration, we employed Biolog's Mitochondrial Function Assay to measure the capacity of cellular machinery to utilize intermediate metabolic substrates of glycolysis and the TCA cycle. Using hierarchical clustering, we found that the metformin and

combination treatments clustered with the uninfected cells, where 2-deoxy-glucose and infected cells clustered together (Fig. 2.9A). In the infected groups' metformin and combination treatments utilized

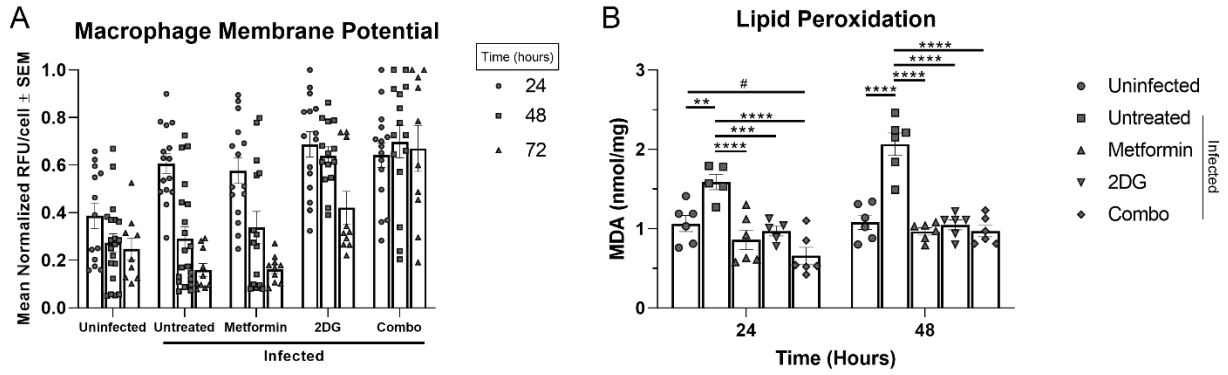

Figure 2.8. Mitochondria integrity stabilized with combination treatment in infected GpBMMϕ. With combination treatment GpBMMϕ maintained mitochondria membrane potential over the 72 hours of infection; in contrast, the untreated group demonstrated a significant collapse in potential over the same time, evidence of mitochondrial dysfunction (A). Total cell malondialdehyde concentrations were significantly elevated in untreated cells, which was prevented in all treatment groups, reducing damaging ROS production from infection (B). Mitochondria membrane potential was measured utilizing a 96-well format, and cells were infected and treated for specified time points before being stained with tetramethylrhodamine methyl ester perchlorate. Fluorescent values were normalized to cell numbers, and a ratio was determined based on the maximum plate value. Two-factor ANOVA analyzed data with Tukey's correction for multiple comparisons; n = 7 – 20 (A). Malondialdehyde concentrations were detected in infected or uninfected cells, treated for specified time points, and assayed per the manufacturer's instructions. Values were normalized to protein concentration. Data were analyzed by two-factor ANOVA with Tukey's correction for multiple comparisons; n = 5 – 6 (B). ** $p \leq 0.01$, *** $p \leq 0.001$, **** $p \leq 0.001$.

nearly all the substrates at a higher level (Fig. 2.9A). Key differences were found between the utilization of cis-aconitic acid, succinic acid, citrate acid, and fumarate between untreated and treated infected groups (Supplemental T2). Finally, substrates were grouped to visualize differences in metabolic pathways. The combination and 2-deoxy-glucose treatments trended a greater utilization in all pathways than untreated. Metformin had fewer differences than untreated; however, they were found in the TCA, amino acid, and ketone pathway substrates (Fig. 2.9B). Together, these data show that combination treatment confers the greatest protection from *M. tuberculosis*-induced mitochondrial damage.

Combination treatment reduces necrosis and pyroptosis while increasing apoptosis in infected cells.

Finally, we examined cell death mechanisms to link metabolism, mitochondrial function, and bacterial clearance. *M. tuberculosis* is known to exploit cell death to promote replication and avoid the immune response. Macrophages undergoing necrosis have been shown to harbor replicating bacteria, where apoptosis promotes *M. tuberculosis* death and increased antigen presentation through

phagocytosis of apoptotic bodies. By 12 hours, combination and 2-deoxy-glucose treatments had a significantly higher percentage of apoptotic cells than untreated, 4.8% and 6.9%,

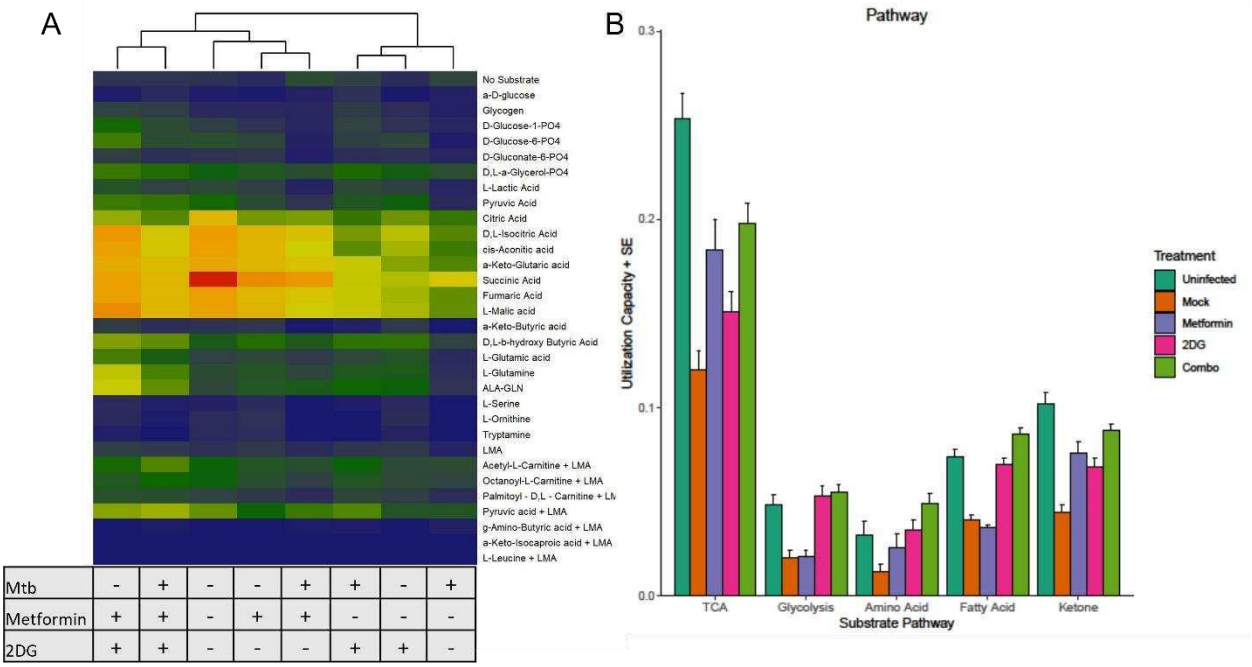

Figure 2.9. **Interventions preserve metabolic utilization capacity during infection.** At 24 hours post-infection, GpBMMϕ had significantly reduced capacity to utilize nearly all substrates. Hierarchical clustering demonstrated that metformin and combination-treated cells with or without infection clustered with uninfected cells, where 2-deoxy-glucose and untreated groups clustered together (A). Substrates were clustered by metabolic pathways, and infected treated cells demonstrated a greater ability to utilize the TCA, amino acid, and ketone pathways. Combination-treated infected cells saw increased utilization for all substrates, further evidence that combination treatment preserves mitochondrial machinery and function (A). GpBMMϕ cells were infected or not with and without treatments for 24 hours. Fifty thousand cells were plated per well and lyzed with Saponin. Plates were read every 15 minutes for four hours at 590nm. Data were analyzed with R. Second-degree polynomial interaction models were constructed per substrate, and the slope was used as the value in the heat-map; n = 3 – 5 with three replicates per n.

respectively, or metformin, 3.0%, and 5.2%, respectively. Untreated cells displayed elevated caspase 1+ cells (Fig. 2.10A), a marker for pyroptosis, a pro-inflammatory programmed cell death mechanism connected to more severe disease. By 24 hours, Caspase 1+ cells comprised approximately 75% of untreated and metformin-treated cells, where 2-deoxy-glucose treatment had 47.8% and combination treatment was lower at 39.2% (Fig. 2.10B).

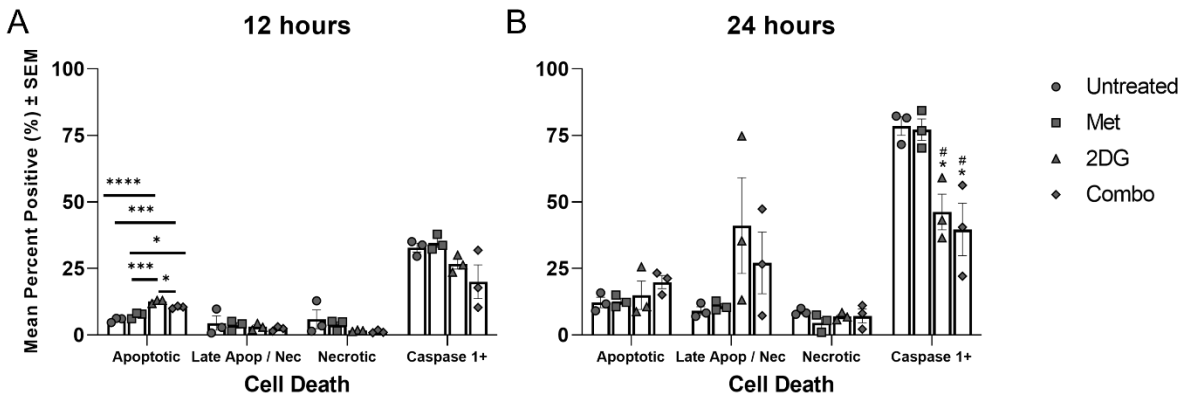

Figure 2.10. Combination treatment increased antimicrobial while decreasing pro-inflammatory mechanisms of cell death. Mycobacterium tuberculosis infection exploits necrotic cell death for replication, while apoptosis promotes bacterial clearance and antigen presentation. Combination treatment displayed a 2-fold increase in apoptosis, then GpBMMϕ cells were infected for 12 hours (A). By 24 hours, late apoptotic cells had an approximately 4-fold increase. Additionally, there was a significant decrease in Caspase 1+ cells over 24 hours compared to untreated cells, a pro-inflammatory cell death mechanism (B). GpBMMϕ cells were infected and treated or remained uninfected and were stained with Annexin V, Zombie NIR, and FLICA 660 Caspase-1 probe. Data were collected with the Aurora Spectral Cytometer and analyzed using FlowJo software. n = 3; *, # $p \leq 0.05$, *** $p \leq 0.001$, *** $p \leq 0.0001$.

DISCUSSION

Tuberculosis remains a global health threat even with recent progress, and the SARS-CoV-2 pandemic has demonstrated how fragile these gains are [95]. Developing new antibiotics is laborious and expensive, inevitably leading to new resistant strains [96]. Current work has emerged emphasizing the connection between metabolism and immune function, and host-directed therapies have emerged as a possible adjunctive option to lengthy treatment regimens. Here we used the guinea pig and macrophage model to characterize the activity of metformin, 2-deoxy-glucose, and combination treatment. We show here that the metabolic switch to glycolysis is insufficient to control disease, and modulation of oxidative phosphorylation is essential.

The balance between glycolysis and oxidative phosphorylation, the two major energy production pathways, is vital to cell function, and manipulation leads to desirable and undesirable outcomes during *M. tuberculosis* infection. Metformin's immune-modulatory effect is partly due to the partial inhibition of complex I of the electron transport chain, which regulates cell differentiation, growth, and function in numerous cell types [97]. Metformin has been reported to positively affect disease outcomes during *M. tuberculosis* infection [92, 98]; however, we found that metformin administered during the peak of the adaptive immune response leads to a more severe lesion burden in the guinea pig model. This increase in disease burden may be due to a poorly timed down-regulation of the immune response. Consistent with previous reports on the effects of 2-deoxy-glucose preferentially affecting infiltrating macrophages, shown to control bacterial burden better than resident macrophages and reduced anti-inflammatory pathways [99, 100], an increased disease burden was found with 2-deoxy-glucose inhibition of glycolysis. These findings and the effects of treatments on infected GpBMMϕ metabolism (Fig. 2.4A-B) demonstrate that inhibition of a single pathway is compensated by the other. In contrast, the damping of both pathways led to a similar disease burden to untreated animals implying that the dual treatment resulted in a null effect; however, histology analysis demonstrated healing within the lung in the form of increased fibrous connective tissue surrounding primary lesions. A further nuanced histopathologic analysis and additional studies are needed to determine the temporal effects metformin and 2-deoxy-glucose in combination have on disease progression.

The role of the mitochondria is more than energy generation. It generates ROS for activation and iNOS, antimicrobial precursors, and Krebs Cycle intermediates for signaling [101]. *M. tuberculosis* disruption of mitochondria function is well documented [102, 103] and supported here in the collapse of the mitochondrial membrane potential, increased proton leak, and reduced spare capacity in the GpBMMϕ model. In single treatments of metformin and 2-deoxy-glucose, mixed results demonstrated an unhealthy mitochondrion; however, the combination of metformin and 2-deoxy-glucose prevented mitochondrial damage due to infection in GpBMMϕ. The key was their ability to maintain membrane potential throughout the study; in addition, we found that infected cells had a reduced capacity to utilize intermediates of glycolysis and the tricarboxylic acid cycle. Again, the combination-treated cells had improved utilization. Specifically, the reduced utilization of citric acid for ATP production demonstrates the potential for increased production of itaconate and iNOS, known antimicrobial compounds. Again, in the combination treatment compared to the uninfected, the reduction in succinic acid utilization implies a shift from energy to cell signaling. The GpBMMϕ still requires ATP, and here we show its sourced from amino and fatty acids. Supporting this energy source may lead to increased host viability and bacterial killing.

The mitochondria are ultimately connected to the fate of the cell. Necrotic cell death is generally detrimental to bacterial control [104], and a high bacterial burden is linked to pyroptosis [102] with poor clinical outcomes in patients [105]. Oxidative stress contributes to these modes of cell death in untreated cells, which one could hypothesize is from a high mitochondrial proton leak resulting in increased cell damaging ROS. Tuberculosis is a chronic inflammatory disease with damage produced from a robust ineffective immune response during active disease. Here we found that combination treatment reduces pyroptosis, a pro-inflammatory mechanism of cell death. Moreover, increased apoptosis here leads to increased bacterial death. This study shows that the dual treatment of metformin and 2-deoxyglucose can increase apoptosis, simultaneously reducing necrosis and pyroptosis, limiting bacteria in GpBMMϕ, which may explain the improved disease outcome *in vivo*.

This study's limitation is the single time point and low sample size in the *in vivo* experiment. Moving forward, it is necessary to understand the temporal effects of the combination treatment on disease burden to determine the efficacy of the treatment. Additionally, a nuanced approach to histopathological image analysis would be performed to evaluate the observed healing (fibrosis).

Moreover, with the combination treatment, an understanding of reduced ATP output resulting in improved disease outcomes requires a deeper investigation into the metabolism of infected GpBMMϕ and animal model may illuminate additional druggable targets. Utilizing isotope tracing and metabolomics may reveal additional pathways for successful treatment outcomes.

REFERENCES

1. Organization, G.W.H., *Global tuberculosis report 2022.* 2022.
2. Organization, G.W.H., *Global tuberculosis report 2019*. 2019.
3. Dean, A.S., et al., *25 years of surveillance of drug-resistant tuberculosis: achievements, challenges, and way forward.* Lancet Infect Dis, 2022. **22**(7): p. e191-e196.
4. Kwan, C.K. and J.D. Ernst, *HIV and tuberculosis: a deadly human syndemic.* Clin Microbiol Rev, 2011. **24**(2): p. 351-76.
5. Administration, U.S.F.D. *FDA approves new drug for treatment-resistant forms of tuberculosis that affects the lungs*. August 14, 2019.
6. Mallick, J.S., et al., *Acquired bedaquiline resistance during the treatment of drug-resistant tuberculosis: a systematic review.* JAC Antimicrob Resist, 2022. **4**(2): p. dlac029.
7. de Martino, M., et al., *Immune Response to Mycobacterium tuberculosis: A Narrative Review.* Front Pediatr, 2019. **7**: p. 350.
8. Zong, Z., et al., *Relapse Versus Reinfection of Recurrent Tuberculosis Patients in a National Tuberculosis Specialized Hospital in Beijing, China.* Front Microbiol, 2018. **9**: p. 1858.
9. Russell, D.G., C.E. Barry, 3rd, and J.L. Flynn, *Tuberculosis: what we don't know can, and does, hurt us.* Science, 2010. **328**(5980): p. 852-6.
10. Queval, C.J., R. Brosch, and R. Simeone, *The Macrophage: A Disputed Fortress in the Battle against Mycobacterium tuberculosis.* Front Microbiol, 2017. **8**: p. 2284.
11. Ehlers, S. and U.E. Schaible, *The granuloma in tuberculosis: dynamics of a host-pathogen collusion.* Front Immunol, 2012. **3**: p. 411.
12. Elkington, P., et al., *Understanding the tuberculosis granuloma: the matrix revolutions.* Trends Mol Med, 2022. **28**(2): p. 143-154.
13. Mahamed, D., et al., *Intracellular growth of Mycobacterium tuberculosis after macrophage cell death leads to serial killing of host cells.* Elife, 2017. **6**.
14. Wynn, T.A., A. Chawla, and J.W. Pollard, *Macrophage biology in development, homeostasis and disease.* Nature, 2013. **496**(7446): p. 445-55.
15. Davies, L.C., et al., *Tissue-resident macrophages.* Nat Immunol, 2013. **14**(10): p. 986-95.
16. Means, T.K., et al., *Human toll-like receptors mediate cellular activation by Mycobacterium tuberculosis.* J Immunol, 1999. **163**(7): p. 3920-7.
17. Uribe-Querol, E. and C. Rosales, *Control of Phagocytosis by Microbial Pathogens.* Front Immunol, 2017. **8**: p. 1368.
18. Cohen, S.B., et al., *Alveolar Macrophages Provide an Early Mycobacterium tuberculosis Niche and Initiate Dissemination.* Cell Host Microbe, 2018. **24**(3): p. 439-446 e4.
19. Lam, A., et al., *Role of apoptosis and autophagy in tuberculosis.* Am J Physiol Lung Cell Mol Physiol, 2017. **313**(2): p. L218-L229.
20. Redente, E.F., et al., *Differential polarization of alveolar macrophages and bone marrow-derived monocytes following chemically and pathogen-induced chronic lung inflammation.* J Leukoc Biol, 2010. **88**(1): p. 159-68.
21. Orecchioni, M., et al., *Macrophage Polarization: Different Gene Signatures in M1(LPS+) vs. Classically and M2(LPS-) vs. Alternatively Activated Macrophages.* Front Immunol, 2019. **10**: p. 1084.
22. Russell, D.G., L. Huang, and B.C. VanderVen, *Immunometabolism at the interface between macrophages and pathogens.* Nat Rev Immunol, 2019. **19**(5): p. 291-304.

23. Zhu, J. and C.B. Thompson, *Metabolic regulation of cell growth and proliferation.* Nat Rev Mol Cell Biol, 2019. **20**(7): p. 436-450.
24. Zheng, J., *Energy metabolism of cancer: Glycolysis versus oxidative phosphorylation (Review).* Oncol Lett, 2012. **4**(6): p. 1151-1157.
25. Vander Heiden, M.G., L.C. Cantley, and C.B. Thompson, *Understanding the Warburg effect: the metabolic requirements of cell proliferation.* Science, 2009. **324**(5930): p. 1029-33.
26. Jones, W. and K. Bianchi, *Aerobic glycolysis: beyond proliferation.* Front Immunol, 2015. **6**: p. 227.
27. Martinez-Reyes, I. and N.S. Chandel, *Mitochondrial TCA cycle metabolites control physiology and disease.* Nat Commun, 2020. **11**(1): p. 102.
28. Palmieri, E.M., et al., *Nitric Oxide in Macrophage Immunometabolism: Hiding in Plain Sight.* Metabolites, 2020. **10**(11).
29. Jobgen, W.S., et al., *Regulatory role for the arginine-nitric oxide pathway in metabolism of energy substrates.* J Nutr Biochem, 2006. **17**(9): p. 571-88.
30. Xiao, M., et al., *Inhibition of alpha-KG-dependent histone and DNA demethylases by fumarate and succinate that are accumulated in mutations of FH and SDH tumor suppressors.* Genes Dev, 2012. **26**(12): p. 1326-38.
31. Tannahill, G.M., et al., *Succinate is an inflammatory signal that induces IL-1beta through HIF-1alpha.* Nature, 2013. **496**(7444): p. 238-42.
32. Choi, I., H. Son, and J.H. Baek, *Tricarboxylic Acid (TCA) Cycle Intermediates: Regulators of Immune Responses.* Life (Basel), 2021. **11**(1).
33. Collins, J.M., et al., *TCA cycle remodeling drives pro-inflammatory signaling in humans with pulmonary tuberculosis.* PLoS Pathog, 2021. **17**(9): p. e1009941.
34. Patil, N.K., et al., *Regulation of leukocyte function by citric acid cycle intermediates.* J Leukoc Biol, 2019. **106**(1): p. 105-117.
35. Kelly, B. and L.A. O'Neill, *Metabolic reprogramming in macrophages and dendritic cells in innate immunity.* Cell Res, 2015. **25**(7): p. 771-84.
36. Isaacs, J.S., et al., *HIF overexpression correlates with biallelic loss of fumarate hydratase in renal cancer: novel role of fumarate in regulation of HIF stability.* Cancer Cell, 2005. **8**(2): p. 143-53.
37. Zhu, X., et al., *Itaconic acid exerts anti-inflammatory and antibacterial effects via promoting pentose phosphate pathway to produce ROS.* Sci Rep, 2021. **11**(1): p. 18173.
38. Wang, H., et al., *An essential bifunctional enzyme in Mycobacterium tuberculosis for itaconate dissimilation and leucine catabolism.* Proc Natl Acad Sci U S A, 2019. **116**(32): p. 15907-15913.
39. Galluzzi, L., et al., *Molecular mechanisms of cell death: recommendations of the Nomenclature Committee on Cell Death 2018.* Cell Death Differ, 2018. **25**(3): p. 486-541.
40. Fink, S.L. and B.T. Cookson, *Apoptosis, pyroptosis, and necrosis: mechanistic description of dead and dying eukaryotic cells.* Infect Immun, 2005. **73**(4): p. 1907-16.
41. Tang, D., et al., *The molecular machinery of regulated cell death.* Cell Res, 2019. **29**(5): p. 347-364.
42. Kaczanowski, S., *Apoptosis: its origin, history, maintenance and the medical implications for cancer and aging.* Phys Biol, 2016. **13**(3): p. 031001.
43. Bedoui, S., M.J. Herold, and A. Strasser, *Emerging connectivity of programmed cell death pathways and its physiological implications.* Nat Rev Mol Cell Biol, 2020. **21**(11): p. 678-695.
44. Elmore, S., *Apoptosis: a review of programmed cell death.* Toxicol Pathol, 2007. **35**(4): p. 495-516.
45. Fan, T.J., et al., *Caspase family proteases and apoptosis.* Acta Biochim Biophys Sin (Shanghai), 2005. **37**(11): p. 719-27.

46. Kale, J., E.J. Osterlund, and D.W. Andrews, *BCL-2 family proteins: changing partners in the dance towards death.* Cell Death Differ, 2018. **25**(1): p. 65-80.
47. Brentnall, M., et al., *Caspase-9, caspase-3 and caspase-7 have distinct roles during intrinsic apoptosis.* BMC Cell Biol, 2013. **14**: p. 32.
48. Porter, A.G. and R.U. Janicke, *Emerging roles of caspase-3 in apoptosis.* Cell Death Differ, 1999. **6**(2): p. 99-104.
49. Bergsbaken, T., S.L. Fink, and B.T. Cookson, *Pyroptosis: host cell death and inflammation.* Nat Rev Microbiol, 2009. **7**(2): p. 99-109.
50. Ziegler, U. and P. Groscurth, *Morphological features of cell death.* News Physiol Sci, 2004. **19**: p. 124-8.
51. Choi, M.E., et al., *Necroptosis: a crucial pathogenic mediator of human disease.* JCI Insight, 2019. **4**(15).
52. Russo, H.M., et al., *Active Caspase-1 Induces Plasma Membrane Pores That Precede Pyroptotic Lysis and Are Blocked by Lanthanides.* J Immunol, 2016. **197**(4): p. 1353-67.
53. Wang, M., X. Chen, and Y. Zhang, *Biological Functions of Gasdermins in Cancer: From Molecular Mechanisms to Therapeutic Potential.* Front Cell Dev Biol, 2021. **9**: p. 638710.
54. Festjens, N., T. Vanden Berghe, and P. Vandenabeele, *Necrosis, a well-orchestrated form of cell demise: signalling cascades, important mediators and concomitant immune response.* Biochim Biophys Acta, 2006. **1757**(9-10): p. 1371-87.
55. Dhuriya, Y.K. and D. Sharma, *Necroptosis: a regulated inflammatory mode of cell death.* J Neuroinflammation, 2018. **15**(1): p. 199.
56. Chen, X., et al., *Translocation of mixed lineage kinase domain-like protein to plasma membrane leads to necrotic cell death.* Cell Res, 2014. **24**(1): p. 105-21.
57. Samson, A.L., et al., *MLKL trafficking and accumulation at the plasma membrane control the kinetics and threshold for necroptosis.* Nat Commun, 2020. **11**(1): p. 3151.
58. Srinivasan, L., S. Ahlbrand, and V. Briken, *Interaction of Mycobacterium tuberculosis with host cell death pathways.* Cold Spring Harb Perspect Med, 2014. **4**(8).
59. Velmurugan, K., et al., *Mycobacterium tuberculosis nuoG is a virulence gene that inhibits apoptosis of infected host cells.* PLoS Pathog, 2007. **3**(7): p. e110.
60. Pan, H., et al., *Ipr1 gene mediates innate immunity to tuberculosis.* Nature, 2005. **434**(7034): p. 767-72.
61. Bafica, A., et al., *Host control of Mycobacterium tuberculosis is regulated by 5-lipoxygenase-dependent lipoxin production.* J Clin Invest, 2005. **115**(6): p. 1601-6.
62. Sly, L.M., et al., *Survival of Mycobacterium tuberculosis in host macrophages involves resistance to apoptosis dependent upon induction of antiapoptotic Bcl-2 family member Mcl-1.* J Immunol, 2003. **170**(1): p. 430-7.
63. Balcewicz-Sablinska, M.K., et al., *Pathogenic Mycobacterium tuberculosis evades apoptosis of host macrophages by release of TNF-R2, resulting in inactivation of TNF-alpha.* J Immunol, 1998. **161**(5): p. 2636-41.
64. Donald, P.R., et al., *Droplets, dust and guinea pigs: an historical review of tuberculosis transmission research, 1878-1940.* Int J Tuberc Lung Dis, 2018. **22**(9): p. 972-982.
65. Dharmadhikari, A.S. and E.A. Nardell, *What animal models teach humans about tuberculosis.* Am J Respir Cell Mol Biol, 2008. **39**(5): p. 503-8.
66. Bafica, A., et al., *TLR9 regulates Th1 responses and cooperates with TLR2 in mediating optimal resistance to Mycobacterium tuberculosis.* J Exp Med, 2005. **202**(12): p. 1715-24.
67. Orme, I.M. and D.J. Ordway, *Mouse and Guinea Pig Models of Tuberculosis.* Microbiol Spectr, 2016. **4**(4).

68. Zhan, L., et al., *Animal Models for Tuberculosis in Translational and Precision Medicine.* Front Microbiol, 2017. **8**: p. 717.
69. Carr, A.C. and S. Maggini, *Vitamin C and Immune Function.* Nutrients, 2017. **9**(11).
70. Clark, S., Y. Hall, and A. Williams, *Animal models of tuberculosis: Guinea pigs.* Cold Spring Harb Perspect Med, 2014. **5**(5): p. a018572.
71. Bucsan, A.N., et al., *The current state of animal models and genomic approaches towards identifying and validating molecular determinants of Mycobacterium tuberculosis infection and tuberculosis disease.* Pathog Dis, 2019. **77**(4).
72. Rowe, S. and A.C. Carr, *Global Vitamin C Status and Prevalence of Deficiency: A Cause for Concern?* Nutrients, 2020. **12**(7).
73. Podell, B.K., et al., *Increased severity of tuberculosis in Guinea pigs with type 2 diabetes: a model of diabetes-tuberculosis comorbidity.* Am J Pathol, 2014. **184**(4): p. 1104-1118.
74. Lockridge, J.L., et al., *Analysis of the CD1 antigen presenting system in humanized SCID mice.* PLoS One, 2011. **6**(6): p. e21701.
75. Hiromatsu, K., et al., *Induction of CD1-restricted immune responses in guinea pigs by immunization with mycobacterial lipid antigens.* J Immunol, 2002. **169**(1): p. 330-9.
76. Plumlee, C.R., et al., *Ultra-low Dose Aerosol Infection of Mice with Mycobacterium tuberculosis More Closely Models Human Tuberculosis.* Cell Host Microbe, 2021. **29**(1): p. 68-82 e5.
77. Dharmadhikari, A.S., et al., *Natural infection of guinea pigs exposed to patients with highly drug-resistant tuberculosis.* Tuberculosis (Edinb), 2011. **91**(4): p. 329-38.
78. Behr, M.A., P.H. Edelstein, and L. Ramakrishnan, *Revisiting the timetable of tuberculosis.* BMJ, 2018. **362**: p. k2738.
79. Young, C., G. Walzl, and N. Du Plessis, *Therapeutic host-directed strategies to improve outcome in tuberculosis.* Mucosal Immunol, 2020. **13**(2): p. 190-204.
80. Doncheva, N.T., et al., *Human pathways in animal models: possibilities and limitations.* Nucleic Acids Res, 2021. **49**(4): p. 1859-1871.
81. Scriba, T.J., M.G. Netea, and A.M. Ginsberg, *Key recent advances in TB vaccine development and understanding of protective immune responses against Mycobacterium tuberculosis.* Semin Immunol, 2020. **50**: p. 101431.
82. tuberculosis., R.c.k.c.t.t.t.o.d.-r., *Geneva: World Health Organization*. 2022.
83. Giller, D.B., et al., *Treatment of pulmonary tuberculosis: past and present.* Eur J Cardiothorac Surg, 2018. **53**(5): p. 967-972.
84. Murray, J.F., D.E. Schraufnagel, and P.C. Hopewell, *Treatment of Tuberculosis. A Historical Perspective.* Ann Am Thorac Soc, 2015. **12**(12): p. 1749-59.
85. *STREPTOMYCIN treatment of pulmonary tuberculosis.* Br Med J, 1948. **2**(4582): p. 769-82.
86. Singh, V. and K. Chibale, *Strategies to Combat Multi-Drug Resistance in Tuberculosis.* Acc Chem Res, 2021. **54**(10): p. 2361-2376.
87. Schutz, C., et al., *Corticosteroids as an adjunct to tuberculosis therapy.* (1747-6356 (Electronic)).
88. Böhme, J., et al., *Metformin enhances anti-mycobacterial responses by educating CD8+ T-cell immunometabolic circuits.* Nature Communications, 2020. **11**(1): p. 5225.
89. Chukwunonso Obi, B., et al., *Comparative Study of the Antioxidant Effects of Metformin, Glibenclamide, and Repaglinide in Alloxan-Induced Diabetic Rats.* (2314-6753 (Electronic)).
90. Padmapriydarsini, C., et al., *Randomized Trial of Metformin With Anti-Tuberculosis Drugs for Early Sputum Conversion in Adults With Pulmonary Tuberculosis.* (1537-6591 (Electronic)).
91. Palsson-McDermott, E.M. and L.A.J. O'Neill, *Targeting immunometabolism as an anti-inflammatory strategy.* Cell Res, 2020. **30**(4): p. 300-314.
92. Frenkel, J.D.H., et al., *Metformin enhances protection in guinea pigs chronically infected with Mycobacterium tuberculosis.* Sci Rep, 2020. **10**(1): p. 16257.

93. Box, G.E.P. and D.R. Cox, *An Analysis of Transformations.* Journal of the Royal Statistical Society. Series B (Methodological), 1964. **26**(2): p. 211-252.
94. Tukey, J.W., *Exploratory data analysis*. Vol. 2. 1977: Reading, MA.
95. Pai, M., T. Kasaeva, and S. Swaminathan, *Covid-19's Devastating Effect on Tuberculosis Care - A Path to Recovery.* N Engl J Med, 2022. **386**(16): p. 1490-1493.
96. Gygli, S.M., et al., *Antimicrobial resistance in Mycobacterium tuberculosis: mechanistic and evolutionary perspectives.* FEMS Microbiol Rev, 2017. **41**(3): p. 354-373.
97. Lachmandas, E., et al., *Metformin Alters Human Host Responses to Mycobacterium tuberculosis in Healthy Subjects.* J Infect Dis, 2019. **220**(1): p. 139-150.
98. Singhal, A., et al., *Metformin as adjunct antituberculosis therapy.* Sci Transl Med, 2014. **6**(263): p. 263ra159.
99. Huang, L., et al., *Growth of Mycobacterium tuberculosis in vivo segregates with host macrophage metabolism and ontogeny.* J Exp Med, 2018. **215**(4): p. 1135-1152.
100. Zhao, Q., et al., *2-Deoxy-d-Glucose Treatment Decreases Anti-inflammatory M2 Macrophage Polarization in Mice with Tumor and Allergic Airway Inflammation.* Front Immunol, 2017. **8**: p. 637.
101. Iwasaki, Y., Y. Takeshima, and K. Fujio, *Basic mechanism of immune system activation by mitochondria.* Immunol Med, 2020. **43**(4): p. 142-147.
102. Beckwith, K.S., et al., *Plasma membrane damage causes NLRP3 activation and pyroptosis during Mycobacterium tuberculosis infection.* Nat Commun, 2020. **11**(1): p. 2270.
103. Looney, M.M., et al., *Mycobacterium tuberculosis Infection Drives Mitochondria-Biased Dysregulation of Host Transfer RNA-Derived Fragments.* J Infect Dis, 2021. **223**(10): p. 1796-1805.
104. Lerner, T.R., et al., *Mycobacterium tuberculosis replicates within necrotic human macrophages.* J Cell Biol, 2017. **216**(3): p. 583-594.
105. Stutz, M.D., et al., *Macrophage and neutrophil death programs differentially confer resistance to tuberculosis.* Immunity, 2021. **54**(8): p. 1758-1771 e7.

APPENDICES

Supplemental 1. Early treatment efficacy in PBMC.

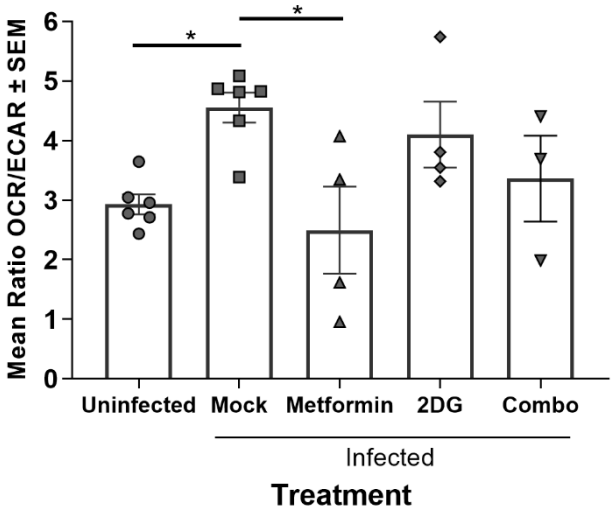

Figure 3.1. Treatment effect in periphery of guinea pigs. Untreated animals displayed elevated OCR compared to uninfected controls. Metformin decreased OCR, however 2-deoxy-glucose failed to decrease ECAR in PBMC two days after treatment began on day 30 post infection. Combination treatment displayed an intermediate effect. PBMC were isolated and OCR and ECAR measured. A ratio of OCR to ECAR was calculated. A one-factor ANONA was used to analysis dataset. A single value was removed from the uninfected groups based on Tukey's IQR k = 7. n = 3 – 6; * $p \leq 0.05$.

Supplemental T1. Tukey's multiple comparisons of early infected GpBMMϕ metabolic data.

OCR					
Tukey's multiple comparisons test	Mean Diff.	95.00% CI of diff.	Significant	Summary	Adjusted P Value
Uninfected vs. Mock	25.91	0.2733 to 51.54	Yes	*	0.0469
Uninfected vs. Metformin	50.25	29.10 to 71.40	Yes	****	<0.0001
Uninfected vs. 2DG	9.629	-14.61 to 33.87	No	ns	0.7474
Uninfected vs. Combo	39.6	17.32 to 61.89	Yes	***	0.0005
Mock vs. Metformin	24.34	4.605 to 44.07	Yes	*	0.0156
Mock vs. 2DG	-16.28	-39.33 to 6.772	No	ns	0.2438
Mock vs. Combo	13.7	-7.212 to 34.61	No	ns	0.2977
Metformin vs. 2DG	-40.62	-57.66 to -23.58	Yes	****	<0.0001
Metformin vs. Combo	-10.64	-22.97 to 1.689	No	ns	0.1084
2DG vs. Combo	29.98	11.29 to 48.66	Yes	**	0.0012
ECAR					
Uninfected vs. Mock	1.895	-6.010 to 9.801	No	ns	0.9363
Uninfected vs. Metformin	-24.98	-34.43 to -15.53	Yes	****	<0.0001
Uninfected vs. 2DG	28.59	20.76 to 36.42	Yes	****	<0.0001
Uninfected vs. Combo	16.88	5.475 to 28.28	Yes	**	0.0024
Mock vs. Metformin	-26.88	-34.63 to -19.12	Yes	****	<0.0001
Mock vs. 2DG	26.69	22.79 to 30.60	Yes	****	<0.0001
Mock vs. Combo	14.98	4.931 to 25.03	Yes	**	0.0035
Metformin vs. 2DG	53.57	45.84 to 61.30	Yes	****	<0.0001
Metformin vs. Combo	41.86	30.75 to 52.97	Yes	****	<0.0001
2DG vs. Combo	-11.71	-21.72 to -1.711	Yes	*	0.0199

Table 3.1. Complete multiple comparison table comparing treatment groups. GpBMMϕ were infected for one hour, treated, and OCR and ECAR was measure for seven hours. Data was normalized to start of treatment. Dataset was analyzed by a mixed-effect REML model with a Geisser-Greenhouse correction. Treatment effect was compared with a Tukey correction for multiple comparisons.

Supplemental T2. A complete description of the analysis of individual substrates and group comparisons.

Differences in Rate of Change in Optical Density - Biolog

Prepared for Dr. Forrest Ackart by Barbara Graham

2019 August 15

Introduction

Optical density (OD) was examined in 96-well plates as a measure of NADH production. Higher OD indicates an increased capacity to use the substrate in the well. The plates were treated with 32 substrates in triplicate across the plate. OD was measured every 15 minutes, beginning at Time = 0, and ending at Time = 4 hours.

Four treatments (Mock, Metformin, 2DG, Combo) were compared under two statuses (Uninfected, Infected). The treatments were compared to each other separately for the Uninfected and the Infected statuses. Similarly, the Uninfected and Infected statuses were compared separately for each treatment.

Results

With the exception of a-D-glucose, L-Serine, and L-Ornithine in the uninfected status, all substrates had at least one comparison of treatments and at least one comparison of infected versus uninfected that had a statistical difference. Rates of change for each treatment are given for the uninfected (Table 1) and the infected (Table 2) statuses. Comparisons for each substrate are given in the following figures showing estimated differences (grey triangle) and 95% confidence interval for the difference. A red dotted line indicates zero, that is, no difference between rates of change.

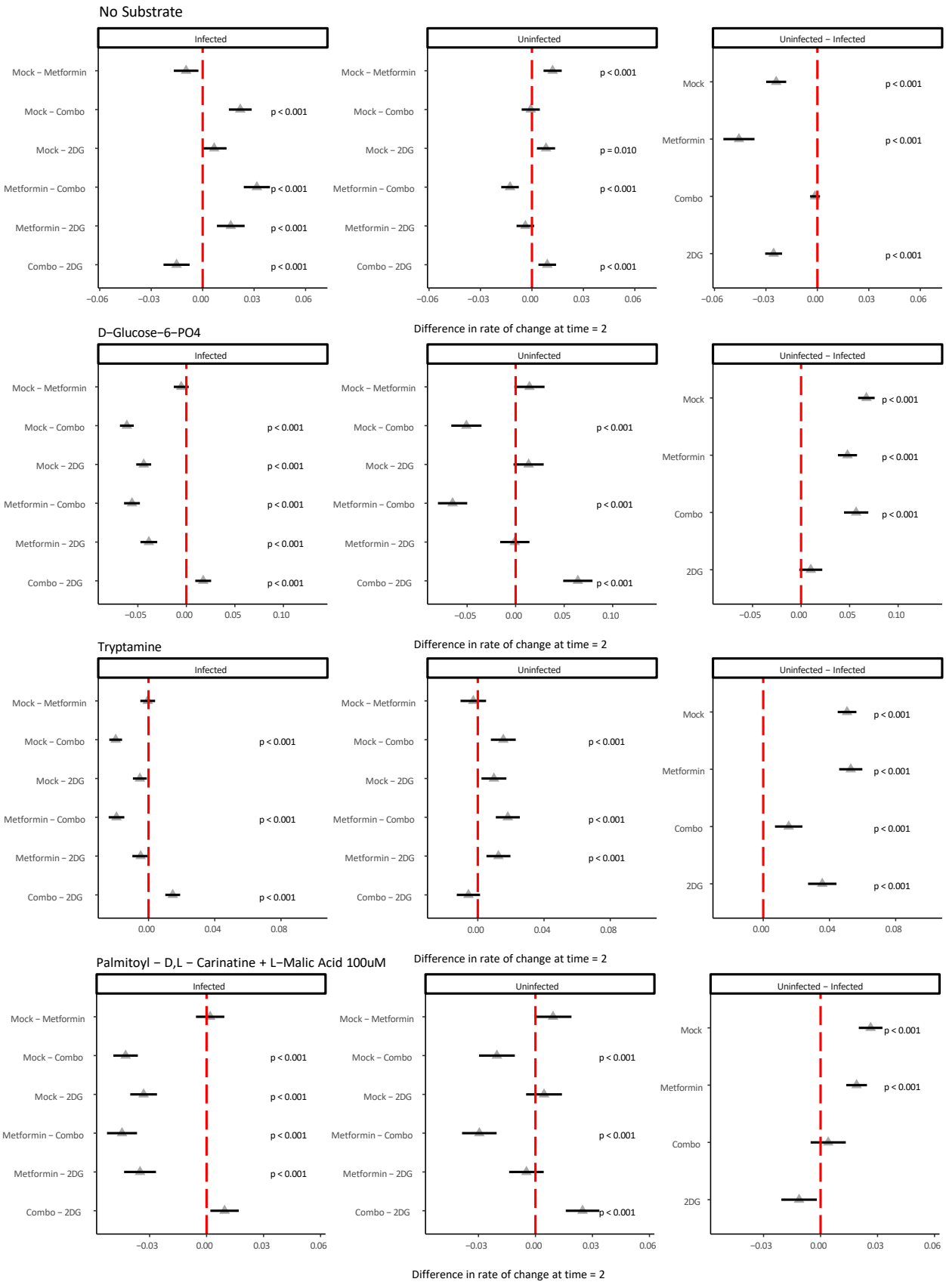
No Substrate
Infected
Uninfected
Uninfected − Infected
Mock − Metformin
Mock − Combo
Mock − 2DG
Metformin − Combo
Metformin − 2DG
Combo − 2DG
p < 0.001
p = 0.010
Mock
Metformin
Combo
2DG
−0.06
−0.03
0.00
0.03
0.06
Difference in rate of change at time = 2
D−Glucose−6−PO4
−0.05
0.00
0.05
0.10
Tryptamine
0.00
0.04
0.08
Palmitoyl − D,L − Carinatine + L−Malic Acid 100uM

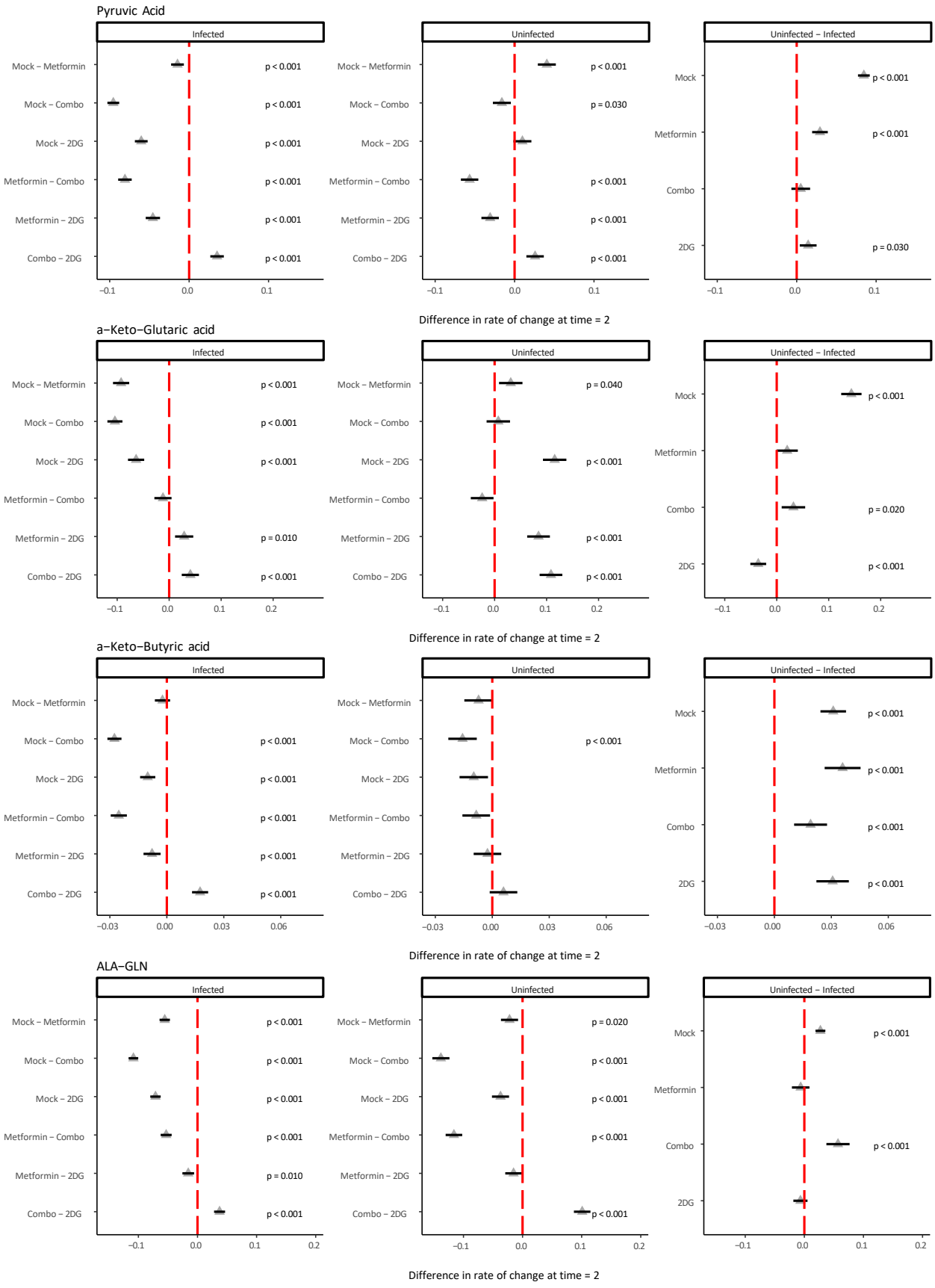
Pyruvic Acid
Infected
Uninfected
Uninfected – Infected
Mock – Metformin
Mock – Combo
Mock – 2DG
Metformin – Combo
Metformin – 2DG
Combo – 2DG
p < 0.001
p < 0.001
p < 0.001
p < 0.001
p < 0.001
p < 0.001
p < 0.001
p = 0.030
p < 0.001
p < 0.001
p < 0.001
p < 0.001
Mock
Metformin
Combo
2DG
p < 0.001
p < 0.001
p = 0.030
−0.1
0.0
0.1
Difference in rate of change at time = 2
a−Keto−Glutaric acid
Infected
Uninfected
Uninfected – Infected
Mock – Metformin
Mock – Combo
Mock – 2DG
Metformin – Combo
Metformin – 2DG
Combo – 2DG
p < 0.001
p < 0.001
p < 0.001
p = 0.010
p < 0.001
p = 0.040
p < 0.001
p < 0.001
p < 0.001
p < 0.001
Mock
Metformin
Combo
2DG
p < 0.001
p = 0.020
p < 0.001
−0.1
0.0
0.1
0.2
Difference in rate of change at time = 2
a−Keto−Butyric acid
Infected
Uninfected
Uninfected – Infected
Mock – Metformin
Mock – Combo
Mock – 2DG
Metformin – Combo
Metformin – 2DG
Combo – 2DG
p < 0.001
p < 0.001
p < 0.001
p < 0.001
p < 0.001
p < 0.001
Mock
Metformin
Combo
2DG
p < 0.001
p < 0.001
p < 0.001
p < 0.001
−0.03
0.00
0.03
0.06
Difference in rate of change at time = 2
ALA−GLN
Infected
Uninfected
Uninfected – Infected
Mock – Metformin
Mock – Combo
Mock – 2DG
Metformin – Combo
Metformin – 2DG
Combo – 2DG
p < 0.001
p < 0.001
p < 0.001
p < 0.001
p = 0.010
p < 0.001
p = 0.020
p < 0.001
p < 0.001
p < 0.001
p < 0.001
Mock
Metformin
Combo
2DG
p < 0.001
p < 0.001
−0.1
0.0
0.1
0.2
Difference in rate of change at time = 2

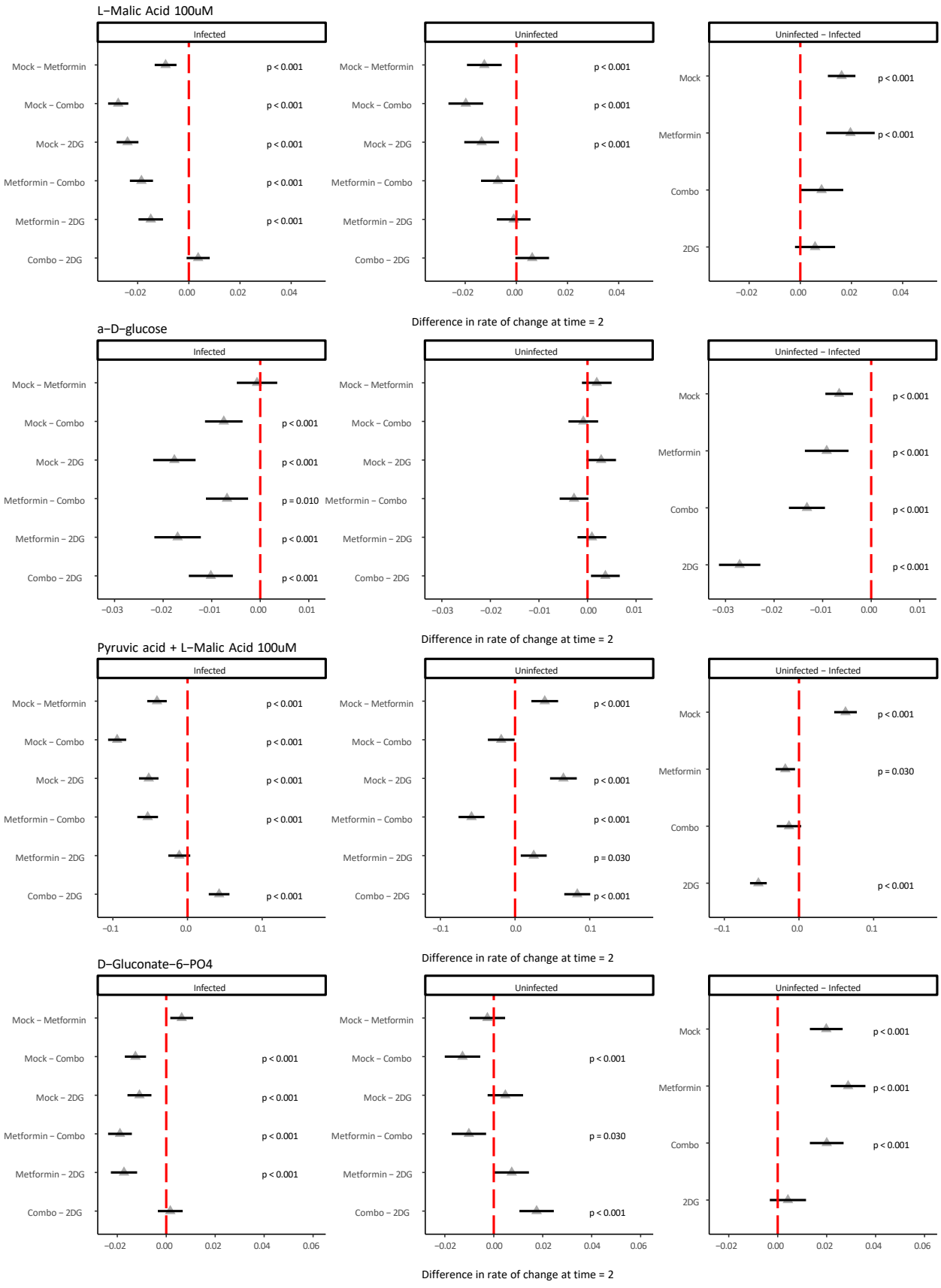
L−Malic Acid 100uM
Infected
Uninfected
Uninfected − Infected
Mock − Metformin
Mock − Combo
Mock − 2DG
Metformin − Combo
Metformin − 2DG
Combo − 2DG
Mock
Metformin
Combo
2DG
p < 0.001
p = 0.010
p = 0.030
−0.02
0.00
0.02
0.04
Difference in rate of change at time = 2
a−D−glucose
−0.03
−0.02
−0.01
0.00
0.01
Pyruvic acid + L−Malic Acid 100uM
−0.1
0.0
0.1
D−Gluconate−6−PO4
0.06

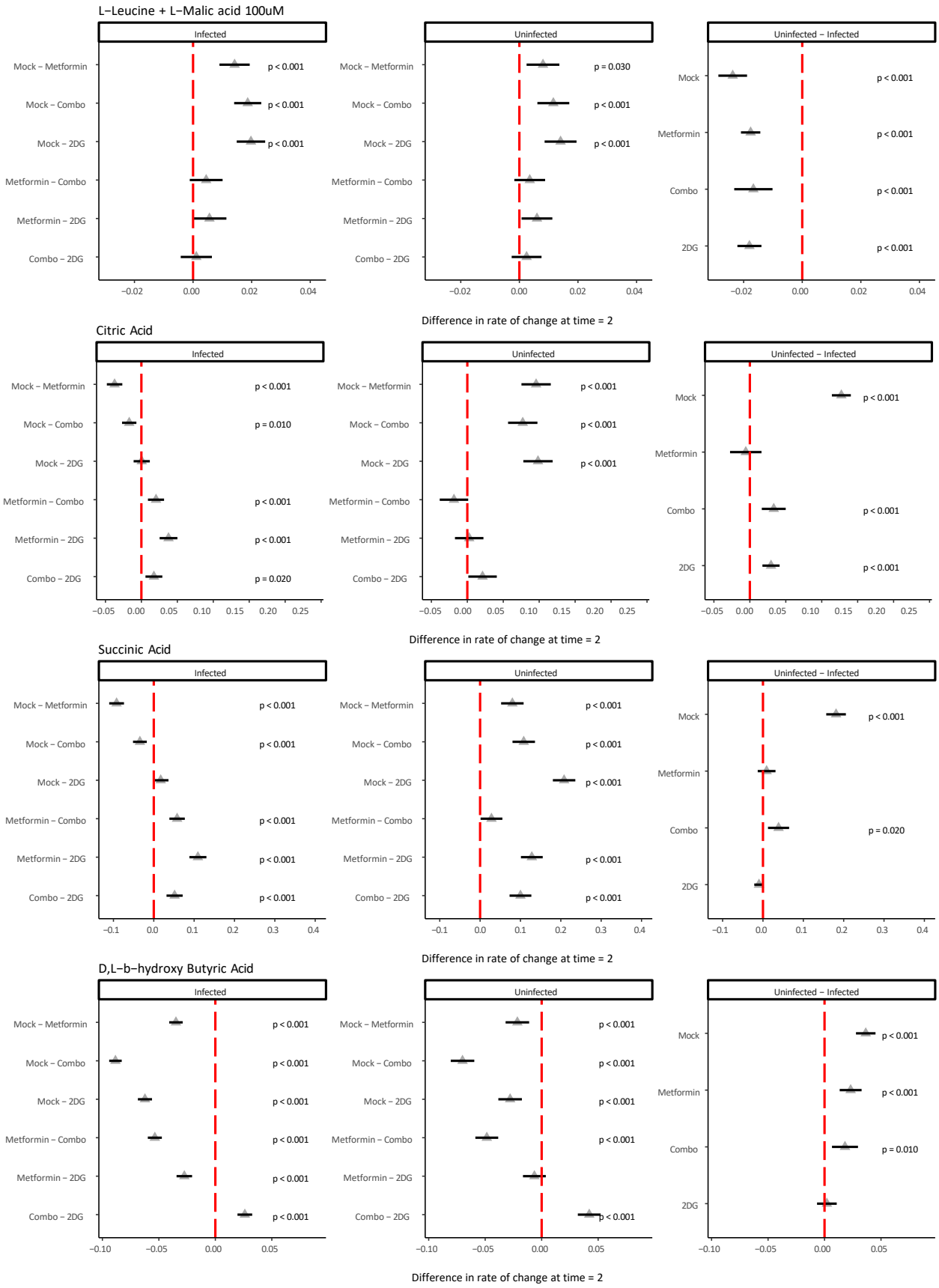
L−Leucine + L−Malic acid 100uM
Infected
Uninfected
Uninfected − Infected
Mock − Metformin
Mock − Combo
Mock − 2DG
Metformin − Combo
Metformin − 2DG
Combo − 2DG
p < 0.001
p < 0.001
p < 0.001
p = 0.030
p < 0.001
p < 0.001
Mock
Metformin
Combo
2DG
p < 0.001
p < 0.001
p < 0.001
p < 0.001
−0.02
0.00
0.02
0.04
Difference in rate of change at time = 2
Citric Acid
Infected
Uninfected
Uninfected − Infected
Mock − Metformin
Mock − Combo
Mock − 2DG
Metformin − Combo
Metformin − 2DG
Combo − 2DG
p < 0.001
p = 0.010
p < 0.001
p < 0.001
p < 0.001
p = 0.020
p < 0.001
p < 0.001
p < 0.001
Mock
Metformin
Combo
2DG
p < 0.001
p < 0.001
p < 0.001
−0.05
0.00
0.05
0.10
0.15
0.20
0.25
Difference in rate of change at time = 2
Succinic Acid
Infected
Uninfected
Uninfected − Infected
Mock − Metformin
Mock − Combo
Mock − 2DG
Metformin − Combo
Metformin − 2DG
Combo − 2DG
p < 0.001
p < 0.001
p < 0.001
p < 0.001
p < 0.001
p < 0.001
p < 0.001
p < 0.001
p < 0.001
Mock
Metformin
Combo
2DG
p < 0.001
p = 0.020
−0.1
0.0
0.1
0.2
0.3
0.4
Difference in rate of change at time = 2
D,L−b−hydroxy Butyric Acid
Infected
Uninfected
Uninfected − Infected
Mock − Metformin
Mock − Combo
Mock − 2DG
Metformin − Combo
Metformin − 2DG
Combo − 2DG
p < 0.001
p < 0.001
p < 0.001
p < 0.001
p < 0.001
p < 0.001
p < 0.001
p < 0.001
p < 0.001
Mock
Metformin
Combo
2DG
p < 0.001
p < 0.001
p = 0.010
−0.10
−0.05
0.00
0.05
Difference in rate of change at time = 2

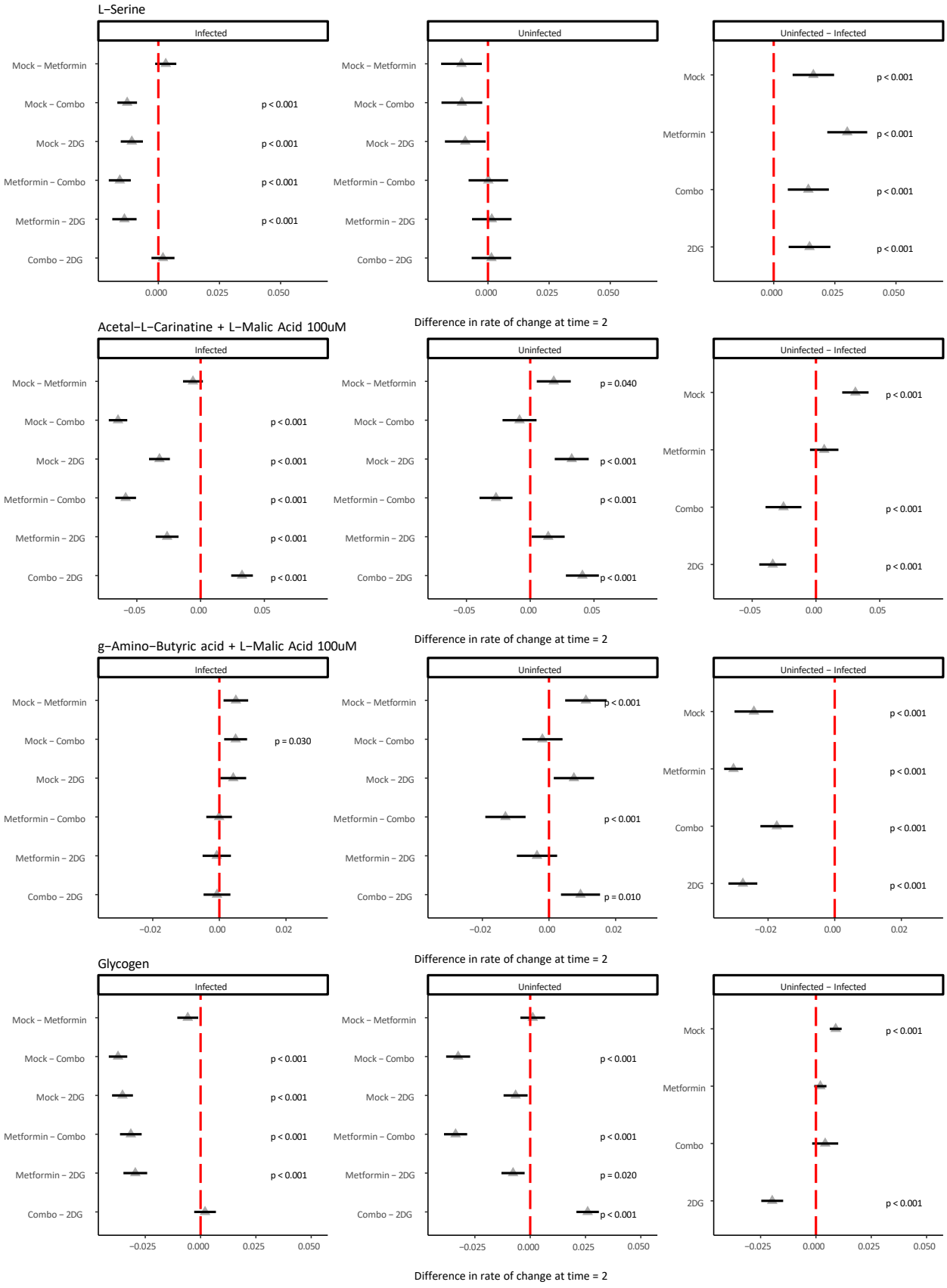
L−Serine
Infected
Uninfected
Uninfected − Infected
Mock − Metformin
Mock − Combo
Mock − 2DG
Metformin − Combo
Metformin − 2DG
Combo − 2DG
p < 0.001
Mock
Metformin
Combo
2DG
0.000
0.025
0.050
Acetal−L−Carinatine + L−Malic Acid 100uM
p = 0.040
−0.05
0.00
0.05
Difference in rate of change at time = 2
g−Amino−Butyric acid + L−Malic Acid 100uM
p = 0.030
p = 0.010
−0.02
0.02
Glycogen
p = 0.020
−0.025

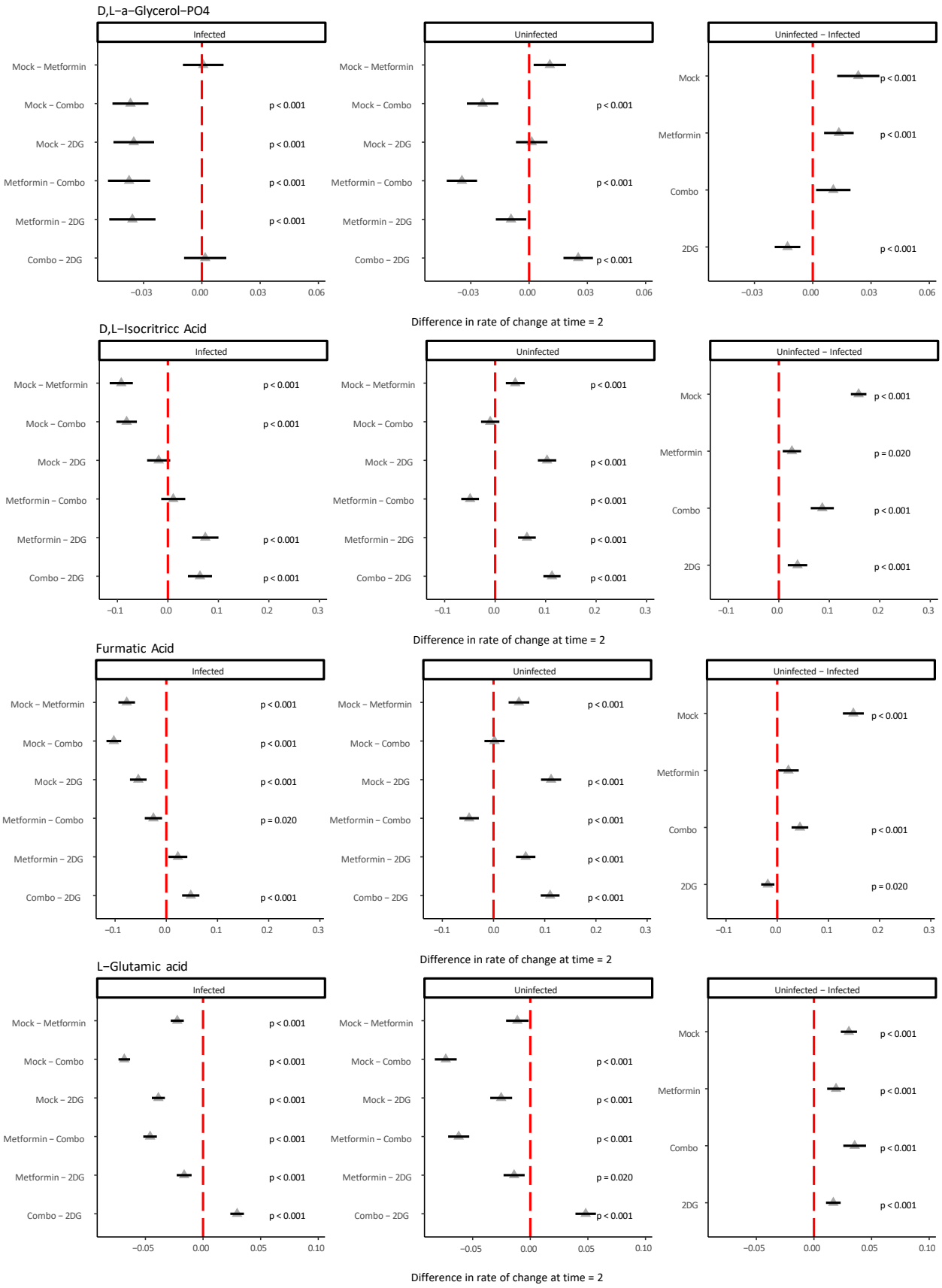
D,L−a−Glycerol−PO4
Infected
Uninfected
Uninfected − Infected
Mock − Metformin
Mock − Combo
Mock − 2DG
Metformin − Combo
Metformin − 2DG
Combo − 2DG
p < 0.001
Mock
Metformin
Combo
2DG
−0.03
0.00
0.03
0.06
Difference in rate of change at time = 2
D,L−Isocritricc Acid
p = 0.020
−0.1
0.0
0.1
0.2
0.3
Furmatic Acid
L−Glutamic acid
−0.05
0.00
0.05
0.10

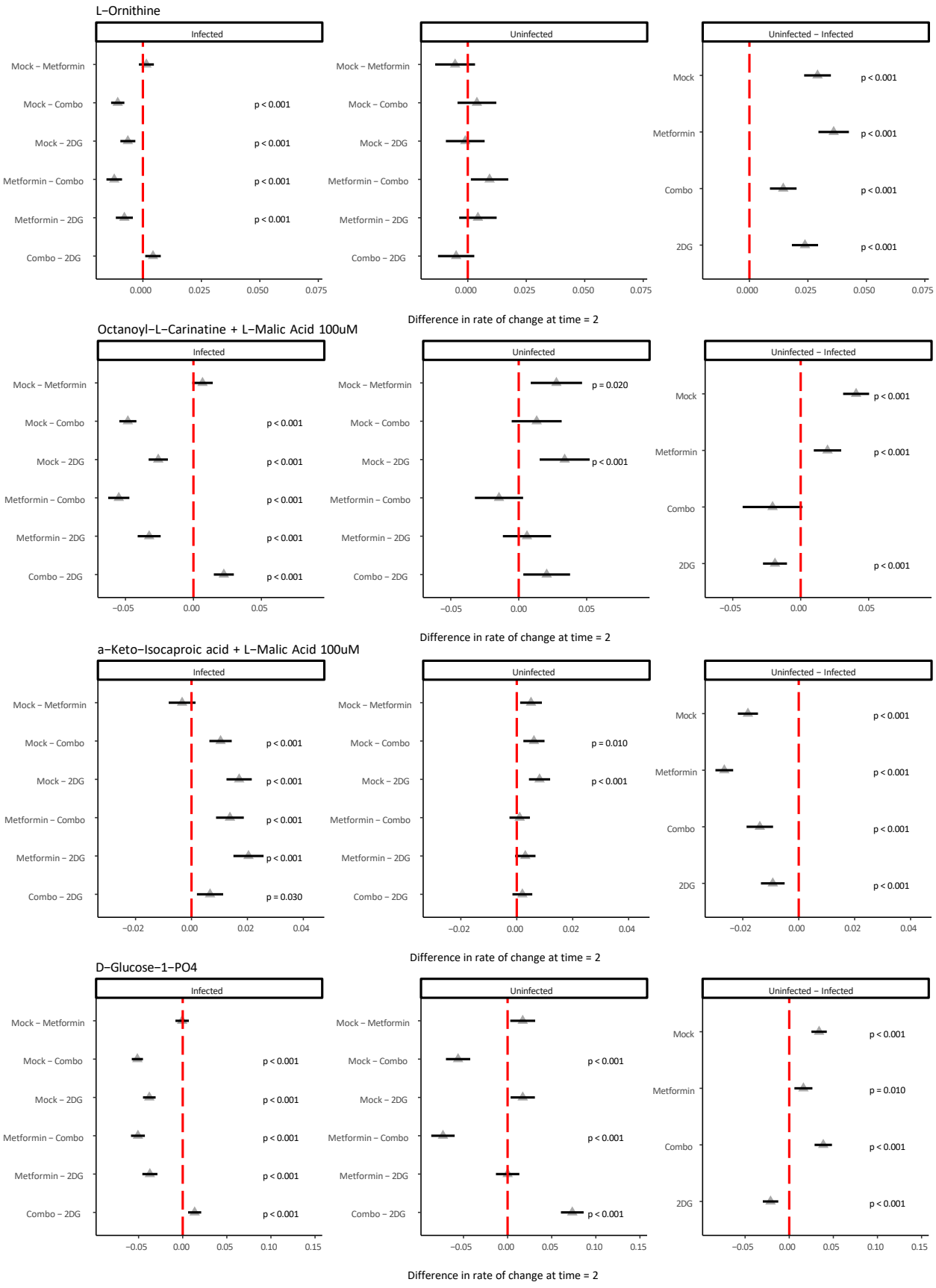
L−Ornithine
Infected
Uninfected
Uninfected − Infected
Mock − Metformin
Mock − Combo
Mock − 2DG
Metformin − Combo
Metformin − 2DG
Combo − 2DG
p < 0.001
Mock
Metformin
Combo
2DG
0.000
0.025
0.050
0.075
Difference in rate of change at time = 2
Octanoyl−L−Carinatine + L−Malic Acid 100uM
p = 0.020
−0.05
0.00
0.05
Difference in rate of change at time = 2
a−Keto−Isocaproic acid + L−Malic Acid 100uM
p = 0.010
p = 0.030
−0.02
0.02
0.04
Difference in rate of change at time = 2
D−Glucose−1−PO4
p = 0.010
0.10
0.15
Difference in rate of change at time = 2

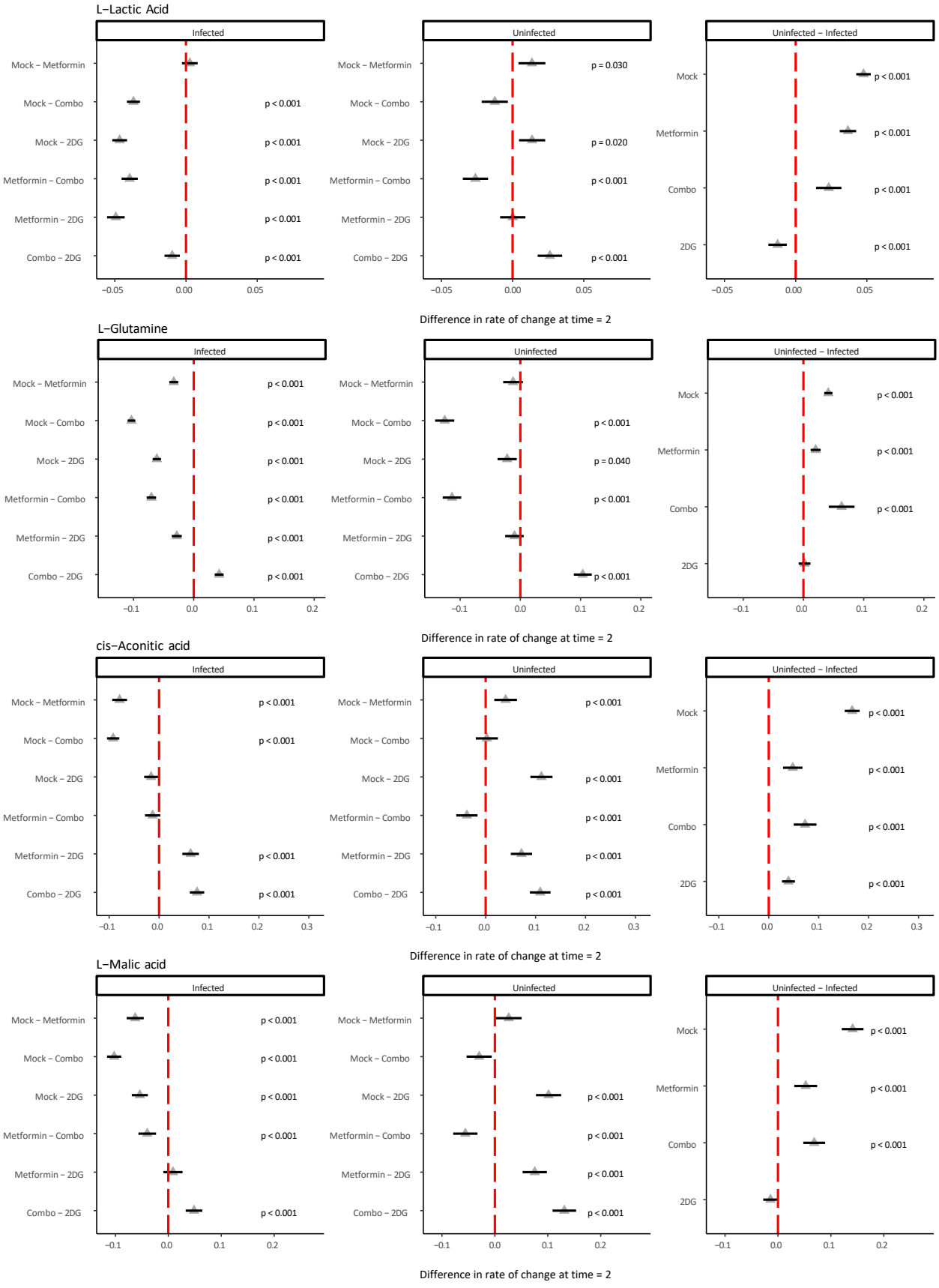
L−Lactic Acid
Infected
Uninfected
Uninfected − Infected
Mock − Metformin
Mock − Combo
Mock − 2DG
Metformin − Combo
Metformin − 2DG
Combo − 2DG
p < 0.001
p = 0.030
p = 0.020
Mock
Metformin
Combo
2DG
−0.05
0.00
0.05
Difference in rate of change at time = 2
L−Glutamine
p = 0.040
−0.1
0.0
0.1
0.2
cis−Aconitic acid
0.3
L−Malic acid

Statistical Methods

All analyses were conducted in R version 3.6.1 (2019-07-05).[1] Interaction second-degree polynomial models were constructed with an interaction on the Time variable alone, and with separate intercepts for each well position × run, using the lme4 package version 1.1.21[2], along with the lmerTest package version 3.1.0 for p-values.[3] The rates of change presented here are the coefficients for the linear effect; Time was centered on 2 (that is, 2 was subtracted from each Time value) so that the coefficients reflected the instantaneous rate of change at Time = 2. Confidence intervals were constructed using the standard errors for the differences as estimated by the models. Degrees of freedom were calculated with Satterthwaite's method[4] for denominator degrees of freedom to account for the unbalanced data. P-values for the differences in rate of change were adjusted within each substrate with a Bonferroni method.[5] Adjustments were made separately for each group represented in a plot, i.e. Infected (6 comparisons), Uninfected (6 comparisons), Uninfected - Uninfected (4 comparisons).

[1] R Core Team. 2019. R: A language and environment for statistical computing. R Foundation for Statistical Computing, Vienna, Austria.
[2] Bates D, Maechler M, Bolker B, Walker S. 2015. Fitting Linear Mixed-Effects Models Using lme4. Journal of Statistical Software 67(1):1–48. doi:10.18637/jss.v067.i01.
[3] Kuznetsova A, Brockhoff PB, Chris- tensen RHB. 2017. lmerTest Package: Tests in Linear Mixed Effects Models. Journal of Statistical Software, 82(13):1–26. doi: 10.18637/jss.v082.i13.
[4] Satterthwaite, FE. 1946. An Approxi- mate Distribution of Estimates of Variance Components. Biometrics Bulletin 2:110–114. doi:10.2307/3002019
[5] Dunn OJ. 1961. Multiple Comparisons Among Means. Journal of the American Statistical Association 56(293):52–64. doi:10.1080/01621459.1961.10482090.

Data Preparation

Well plates were commercially treated with substrates in triplicate across the plate (Table 3). The well positions were categorized as Rep 1, 2, or 3, according to the position on the plate. Rep 1 comprised the first four columns, Rep 2 the second four columns, and Rep 3 the third four columns. OD readings were first adjusted by substrating the values for a "blank." This was conducted separately for each treatment × status combination. Each 96-well plate had two "blank" readings associated with it, unique for each time point. The first "blank" reading was used in rows A, B, C, D, E, and F, and for the substrate in positions G1, G5, and G9 (L-Malic Acid 100 uM). The second "blank" reading was used in the remaining wells in row G, and in row H. As an exception, wells corresponding to No Substrate (A1, A5, A9), used the reading in the first No Substrate well (A1) at time = 0 as the value for "blank." After subtracting the "blank"

values, starting OD (Time = 0) ranged from -0.095 to 0.214. Ending OD (Time = 4) ranged from -0.424 to 1.933.

Limitations

Effects of Run (plate) and of Rep (position on plate) were tested separately, overall for each substrate regardless of treatment or status. OD readings demonstrated differences that appeared to be due to Rep and/or Run for most of the substrates. These effects were not accounted for in the linear models comparing the rates of change at 2 hours. The introduction of additional variables in models to account for Rep and/or Run could compromise the results, since there were too few data points, especially for certain well positions under some treatment × status conditions.

A run effect can be accounted for by making sure that all treatment × status combinations are used in all runs [it's not clear that this was done]. A well-position effect is best handled by randomization of the substrates in the wells. However, this option is not practical, as the plates are commercially produced. It appears that some of the wells were either not measured or failed (for example, Rep 1 for L-Leucine + L-Malic acid 100uM under the Metformin × Infected combination). The missing values may skew the results.

Each substrate was evaluated for difference in rate of change in three different ways: 1) comparison of treatments under uninfected status; 2) comparison of treatments under infected status; 3) comparison of uninfected to infected separately for each treatment. Bonferroni adjustments for multiple comparisons were made within each of these groups, separately for each substrate (the results of uninfected vs infected for all four treatments were adjusted as a group for each substrate). Nonetheless, with 32 substrates the likelihood of finding a statistically significance by chance is increased, and higher p-values (especially those that are close to 0.05) should be viewed with some skepticism.

After subtracting the blank OD values, some of the substrates showed a negative rate of change at 2 hours. The statistical models did not take into consideration whether negative values made sense biologically, but included them as valid measurements.

The experiment was unbalanced, with the number of well positions (reps) and plates (runs) different among the treatment × status combinations. In addition, Mock × Infected was tested with 5 plates (Run 4 and Run 5); the other treatments and statuses were tested with 3 plates.

Additional plots

Additional plots showing the adjusted OD, the modeled values, comparison of rates of change at Time = 2 (shown as slopes/tangent lines), and a visual look at the effect of Run or Rep can be viewed within CSU at this link:

http://rit-03.cvmbs.colostate.edu:3838/BJG_2019-08-05_Ackart-View-Biolog/

Uninfected				
Substrate	2DG	Combo	Metformin	Mock
No Substrate	0.02	0.03	0.02	0.03
D-Glucose-6-PO4	0.06	0.12	0.06	0.07
Pyruvic Acid	0.09	0.12	0.06	0.10
a-Keto-Glutaric acid	0.16	0.27	0.25	0.28
a-Keto-Butyric acid	0.04	0.05	0.04	0.03
ALA-GLN	0.10	0.20	0.08	0.06
L-Malic Acid 100uM	0.04	0.05	0.04	0.03
Pyruvic acid + L-Malic Acid 100uM	0.08	0.16	0.10	0.14
a-D-glucose	0.00	0.01	0.00	0.00
D-Gluconate-6-PO4	0.03	0.05	0.04	0.03
Citric Acid	0.15	0.17	0.15	0.25
Succinic Acid	0.18	0.28	0.31	0.39
D,L-b-hydroxy Butyric Acid	0.12	0.16	0.11	0.09
L-Serine	0.02	0.02	0.02	0.01
Acetal-L-Carinatine + L-Malic Acid 100uM	0.06	0.10	0.08	0.10
g-Amino-Butyric acid + L-Malic Acid 100uM	-0.02	-0.01	-0.03	-0.02
Glycogen	0.03	0.05	0.02	0.02
D,L-a-Glycerol-PO4	0.09	0.12	0.08	0.09
D,L-Isocritricc Acid	0.19	0.30	0.25	0.29
Furmatic Acid	0.18	0.29	0.24	0.29
L-Glutamic acid	0.08	0.13	0.06	0.05
L-Ornithine	0.02	0.02	0.03	0.02
Octanoyl-L-Carinatine + L-Malic Acid 100uM	0.06	0.08	0.07	0.10
a-Keto-Isocaproic acid + L-Malic Acid 100uM	-0.04	-0.04	-0.04	-0.03
D-Glucose-1-PO4	0.03	0.10	0.03	0.05
L-Lactic Acid	0.05	0.08	0.05	0.06
cis-Aconitic acid	0.18	0.29	0.25	0.29
L-Malic acid	0.18	0.31	0.26	0.28
L-Glutamine	0.09	0.19	0.08	0.07
Tryptamine	0.01	0.01	0.03	0.02
Palmitoyl - D,L - Carinatine + L-Malic Acid 100uM	0.05	0.07	0.04	0.05
L-Leucine + L-Malic acid 100uM	-0.04	-0.03	-0.03	-0.02

Table 1: Rate of change at 2 hours under each treatment for Uninfected combinations. Only a-D-glucose, L-Serine, and L-Ornithine had no statistical differences among treatments.

Infected				
Substrate	2DG	Combo	Metformin	Mock
No Substrate	0.05	0.03	0.07	0.06
D-Glucose-6-PO4	0.05	0.07	0.01	0.01
Pyruvic Acid	0.08	0.12	0.03	0.02
a-Keto-Glutaric acid	0.20	0.24	0.23	0.13
a-Keto-Butyric acid	0.01	0.03	0.00	0.00
ALA-GLN	0.10	0.14	0.09	0.03
L-Malic Acid 100uM	0.04	0.04	0.02	0.01
Pyruvic acid + L-Malic Acid 100uM	0.13	0.17	0.12	0.08
a-D-glucose	0.03	0.02	0.01	0.01
D-Gluconate-6-PO4	0.03	0.03	0.01	0.01
Citric Acid	0.12	0.14	0.16	0.12
Succinic Acid	0.19	0.25	0.30	0.21
D,L-b-hydroxy Butyric Acid	0.11	0.14	0.09	0.05
L-Serine	0.01	0.01	-0.01	-0.01
Acetal-L-Carinatine + L-Malic Acid 100uM	0.10	0.13	0.07	0.07
g-Amino-Butyric acid + L-Malic Acid 100uM	0.00	0.00	0.00	0.01
Glycogen	0.05	0.05	0.02	0.01
D,L-a-Glycerol-PO4	0.11	0.11	0.07	0.07
D,L-Isocritricc Acid	0.15	0.22	0.23	0.13
Furmatic Acid	0.20	0.24	0.22	0.14
L-Glutamic acid	0.06	0.09	0.04	0.02
L-Ornithine	0.00	0.00	-0.01	-0.01
Octanoyl-L-Carinatine + L-Malic Acid 100uM	0.08	0.10	0.05	0.05
a-Keto-Isocaproic acid + L-Malic Acid 100uM	-0.03	-0.02	-0.01	-0.01
D-Glucose-1-PO4	0.05	0.07	0.02	0.01
L-Lactic Acid	0.06	0.05	0.01	0.02
cis-Aconitic acid	0.14	0.21	0.20	0.12
L-Malic acid	0.20	0.24	0.20	0.14
L-Glutamine	0.09	0.13	0.06	0.02
Tryptamine	-0.02	-0.01	-0.03	-0.03
Palmitoyl - D,L - Carinatine + L-Malic Acid 100uM	0.06	0.07	0.02	0.03
L-Leucine + L-Malic acid 100uM	-0.02	-0.02	-0.01	0.00

Table 2: Rate of change at 2 hours under each treatment for Infected combinations. All substrates had at least one statistical difference among treatments.

Computing Platform
R version 3.6.1 (2019-07-05) Platform: x86_64-w64-mingw32/x64 (64-bit) Running under: Windows 10 x64 (build 17134)
Matrix products: default
locale: [1] LC_COLLATE=English_United States.1252 [2] LC_CTYPE=English_United States.1252
[3] LC_MONETARY=English_United States.1252 [4] LC_NUMERIC=C
[5] LC_TIME=English_United States.1252
attached base packages: [1] grid stats graphics grDevices [5] utils datasets methods base
other attached packages: [1] kableExtra_1.1.0 gridExtra_2.3
[3] forcats_0.4.0 stringr_1.4.0
[5] dplyr_0.8.3 purrr_0.3.2
[7] readr_1.3.1 tidyr_0.8.3
[9] tibble_2.1.3 ggplot2_3.2.0
[11] tidyverse_1.2.1 tufte_0.5
[13] rmarkdown_1.14
loaded via a namespace (and not attached): [1] tinytex_0.15 tidyse- lect_0.2.5 [3] xfun_0.8 haven_2.1.1
[5] lattice_0.20-38 colorspace_1.4-1 [7] generics_0.0.2 vctrs_0.2.0
[9] htmltools_0.3.6 viridisLite_0.3.0 [11] yaml_2.2.0 utf8_1.1.4
[13] rlang_0.4.0 pillar_1.4.2
[15] glue_1.3.1 withr_2.1.2
[17] modelr_0.1.4 readxl_1.3.1
[19] munsell_0.5.0 gtable_0.3.0
[21] cellranger_1.1.0 rvest_0.3.4
[23] evaluate_0.14 labeling_0.3
[25] knitr_1.24 fansi_0.4.0
[27] broom_0.5.2 Rcpp_1.0.2
[29] scales_1.0.0 backports_1.1.4
[31] formatR_1.7 webshot_0.5.1
[33] jsonlite_1.6 hms_0.5.0
[35] digest_0.6.20 stringi_1.4.3
[37] cli_1.1.0 tools_3.6.1
[39] magrittr_1.5 lazyeval_0.2.2
[41] crayon_1.3.4 pkgconfig_2.0.2
[43] zeallot_0.1.0 xml2_1.2.1
[45] lubridate_1.7.4 assertthat_0.2.1 [47] httr_1.4.1 rstudioapi_0.10
[49] R6_2.4.0 nlme_3.1-141
[51] compiler_3.6.1